Slowing-down times and stopping powers for ~2-MeV μ^+ in low-pressure gases

Masayoshi Senba*
Department of Physics, Dalhousie University, Halifax, Nova Scotia, Canada, B3H 3J5

Donald J. Arseneau, James J. Pan,† and Donald G. Fleming‡
TRIUMF, 4004 Wesbrook Mall, Vancouver, British Columbia, Canada, V6T 2A3
and Department of Chemistry, University of British Columbia, Vancouver, British Columbia, Canada, V6T 1Z1
(Received 14 December 2005; published 9 October 2006)

The times taken by positive muons (μ^+) to slow down from initial energies in the range ~3 to 1 MeV, to the energy of the last muonium formation, ≈10 eV, at the end of cyclic charge exchange, have been measured in the pure gases H_2, N_2, Ar, and in the gas mixtures Ar-He, Ar-Ne, Ar-CF_4, H_2-He, and H_2-SF_6, by the muon spin rotation (μSR) technique. At 1 atm pressure, these slowing-down times, τ_{SD}, in Ar and N_2, vary from ~14 ns at the highest initial energies of 2.8 MeV to 6.5 ns at 1.6 MeV, with much longer times, ~34 ns, seen at this energy in H_2. Similar variations are seen in the gas mixtures, depending also on the total charge and nature of the mixture and consistent with well-established (Bragg) additivity rules. The times τ_{SD} could also be used to determine the stopping powers, dE/dx, of the positive muon in N_2, Ar, and H_2, at kinetic energies near 2 MeV. The results demonstrate that the μ^+ and proton have the same stopping power at the same projectile velocity, as expected from the historic Bethe-Bloch formula, but not previously shown experimentally to our knowledge for the muon in gases at these energies. The energy of the first neutralization collision forming muonium (hydrogen), which initiates a series of charge-exchanging collisions, is also calculated for He, Ne, and Ar. The formalism necessary to describe the stopping power and moderation times, for either muon or proton, in three energy regimes—the Bethe-Bloch, cyclic charge exchange, and thermalization regimes—is developed and discussed in comparison with the experimental measurements reported here, and elsewhere. The slowing-down times through the first two regimes are controlled by the relevant ionization and charge-exchange cross sections, whereas the final thermalization regime is most sensitive to the forwardness of the elastic scattering cross sections. In this regime the slowing-down times (to kT) at nominal pressures are expected to be ≲100 ns.

DOI: 10.1103/PhysRevA.74.042708 PACS number(s): 34.50.Bw, 36.10.Dr, 32.10.Fn

I. INTRODUCTION

The slowing down and thermalization of an energetic particle in matter is relevant to the fields of atomic, nuclear, and particle physics, and to other related fields of science, including radiation and hot-atom chemistry. It is often important to know (i) how long it takes to slow down and stop energetic particles in matter, (ii) what the final products are after this thermalization, and (iii) the energies at which these final products are formed. An understanding of slowing-down times and energy-loss mechanisms at *low* energies is also important in the production of slow muon beams [1,2] and muonic hydrogen isotopes [3] in measurements of the Barkas effect [4], particularly comparing μ^+ and μ^- stopping powers [5], in linear energy transfer (LET) and radiation chemistry studies [6–10], as well as in a variety of muon spin rotation (μSR) studies in both gases [11–19] and in condensed phases [7–10,20,21]. In all these environments, it is important to distinguish between thermal and epithermal processes, mandating, therefore, an understanding of the relevant slowing-down processes. Of fundamental interest as well is the opportunity to test scaling laws in both charge exchange and energy moderation cross sections, and hence in the stopping power, dE/dx, by comparing positive muons and protons at the same velocities [1,22], as in previous comparisons of the stopping powers for protons and deuterons where velocity scaling has been established to better than 0.5% [23–25]. To further investigate these issues, the μSR technique [9,14,15] has been used to measure the slowing down times for positive muons in various gases—the time during which a muon is slowed from its initial "MeV" kinetic energy down to ~10 eV by collisions with the gas.

During its slowing-down processes in matter, the positive muon forms the muonium atom ($Mu=\mu^+e^-$) [2,9–11,14–16,20,21,26–30], its bound state with an electron. Since muonium has essentially the same size and ionization potential as hydrogen, it is regarded as an ultralight isotope of H ($m_H=8.88m_{Mu}$) and has been used accordingly to investigate isotope effects in chemical reactions, both thermal rate constants [12,31–33] and hot atom "yields" [13,14,34], and in thermally averaged spin-exchange cross sections for gas-phase collisions [15,19,35]. In studies of this nature the assumption of a thermalized muon ensemble is tacitly made, meaning that the total slowing-down time is assumed to be much shorter than typical μs relaxation rates. The present measurements provide convincing proof of the validity of this assumption and support as well recent rf-μSR measurements demonstrating prompt Mu formation in gases [11].

*Corresponding author. Email address: msenba@dal.ca
†Present address: Smart&Bigger, Law Offices, Toronto, ON, Canada.
‡Corresponding author. Email address: flem@triumf.ca

The slowing-down time of muons in the gas phase is determined by measuring the muonium precession phase in a μSR experiment, first demonstrated in Ar [36]. The present paper brings the method outlined in Ref. [36] to fruition with much more extensive measurements of slowing-down times in the pure gases H_2, D_2, N_2, and Ar, and in the mixtures Ar-He, Ar-Ne, Ar-CF_4, and H_2-He. These are the *only direct measurements* of slowing-down times for positive muons in any environment to the best of our knowledge. They also provide a method for determining the stopping power of ~1-MeV μ^+ beams in gases.

In addition to these measurements, calculations are also presented which describe the slowing-down process, both in the energy regime studied experimentally (~1 MeV–10 eV) and in the final thermalization regime at energies below ~10 eV, thus fully bridging the gap between high energies and thermal distributions. Calculations of this nature allow a determination of the *total* slowing-down time in the gas, providing an important perspective relevant to discussions of muon interactions and thermalization times in dense media [6–8,10,21,37] as well as providing a basis for discriminating between hot and thermal reactive processes of the Mu atom [13,34].

II. SLOWING DOWN AND THERMALIZATION

The slowing down of positively charged pointlike particles in gases, over wide energy ranges, notably here for the positive muon [10,11,14,16,26–30] and proton [8,38–42], can be divided roughly into the following three energy or time stages or regimes: (i) Bethe-Bloch ionization, (ii) cyclic charge exchange, and (iii) final thermalization, to $3/2kT$. In this work the measured *slowing-down time* (SD time) is defined by the time the energetic particle spends in the Bethe-Bloch *plus* cyclic charge exchange regimes, but *not* the final thermalization regime. This latter time, though, is of considerable importance to comparisons with μSR data in both gases and condensed phase environments, and is addressed here by specific calculations.

In the first [Bethe-Bloch (BB)] regime, kinetic energy loss is primarily the result of ionization and electronic excitation processes, in any environment [6,8,38,40,43–46]. In the second [charge-exchange (CE)] regime, the positive particle spends part of its time as a neutral atom, muonium or hydrogen, and emerges from this regime either as the atom or remaining as a bare μ^+ (or p^+), prior to entering the third, "thermalization," regime. The distribution of muons (protons) among charge states at this stage depends crucially on competition between electron capture and loss processes, as well as energy-moderating cross sections, near the end of cyclic charge exchange [2,14–16,26–28,30,38], as outlined in more detail below.

In molecular gases, these charge state fractions may be changed further by reactive (hot atom) processes [9,13,14,34] to give the measured (gas phase) Mu and diamagnetic fractions in gas-phase μSR experiments; i.e., at observation times *after* thermalization [16–18,47,48]. In dense gases or in condensed phases, the situation is further complicated by "spur effects" [2,6,8–10,20,21,37,47] which can take place over a range of times [10,21], further mandating the importance of knowing SD times and stopping power (LET) in low density environments. Noteworthy here is the distinction between these μSR experiments, where the positive muon actually *stops* in its environment, and most studies of the energy loss of protons (and other ions), which is invariably measured at specific incident energies in particle *transmission* experiments [38,41,42,45].

A. Bethe-Bloch regime and dE/dx

During this regime, the electronic energy loss of a charged particle is well described by the (historic) Bethe-Bloch stopping-power formula [40,44–46,49,50] (which is embodied as well in the much more recent Sigmund-Schinner binary collision theory for the stopping of both heavy ions [51] and, more relevant here, light ions [43]),

$$-\frac{dE}{dx} = \frac{4\pi e^4 z_p^2 Z_T n}{m_e v^2} L(v), \tag{1}$$

where n is the number density of the (target) moderator, z_p is the charge of the projectile, Z_T is the atomic number of the target, v is the projectile velocity (speed), e and m_e are the charge and mass of the electron, respectively, and $L(v)$ is the "stopping number" which includes shell corrections [40,44,52] and additional corrections for the Bloch, Barkas, and relativistic terms [5,40,44,45,50]. For nonrelativistic point (heavy) particles at MeV energies, of interest here, and ignoring the few percent contributions from the Bloch and Barkas terms at such energies [44,45], $L(v)$ can be written as

$$L(v) = \ln(2m_e v^2/I) - C(v)Z_T, \tag{2}$$

where the quantity I is the mean excitation energy of electrons in the medium and $C(v)/Z_T$ is a sum of shell corrections to account for a differing participation of inner and outer shell electrons in the stopping process at different energies. These have been calculated by various assumptions through the years, recently by Bichsel for protons and α particles in solids [44], complimenting earlier studies by Bichsel and Porter in gases [40] and, as used here, by Oddershede and Sabin, in the elements up to $Z_T=36$ [52].

It is noted that the electronic stopping-power formula of Eq. (1) has no explicit projectile mass dependence and, for a given target molecule, depends only on velocity (speed) v, a feature that can be described as "velocity scaling" in comparing stopping powers for charged particles of different masses [1,14–16,22–25]. Shiomi-Tsuda *et al.* [23] concluded, to a high degree of accuracy (0.35%), that there was no difference in stopping powers for equivalent-velocity proton and deuteron energies in several metal targets, consistent with earlier comparisons by Andersen *et al.* [24] and Andersen and Ziegler down to 100 keV [39]. This was subsequently confirmed by Bichsel and Inokuti [25], who also investigated specific nuclear mass contributions to the stopping power (these are enhanced for the muon but at far too low a level to be seen in the present experiments). Earlier, Bichsel and Porter [40] and Reiter *et al.* [42] had examined stopping powers for protons and α particles in gases, at proton energies $\gtrsim$400 keV, and found little or no mass depen-

dence outside experimental (~2%) error, consistent with earlier and more accurate experiments by Andersen *et al.* [24] and more recent comparisons by Bichsel in Si and Al [44]. Larger deviations were seen, though, in a separate study by Reiter *et al.* in halogenetated gases [53], which may be partly due to deviations from "Bragg's rule" (see below). At lower energies, charge exchange, an important aspect of the present experiment, begins to play a role, reducing the effective charge of the projectile [24,40,43,49,51], such that α and proton stopping powers can deviate significantly from the expected ratio $(Z_{He}/Z_H)^2=4$ at the same velocity [40,53], seen as well for low-energy (8 keV) deuterons [54].

The above comparisons involve changing the projectile mass by factors of 2 or 4. In principle, a more stringent test of the mass independence of the (electronic) stopping power can be made by comparing the positive muon with the proton, which differ by a factor of 9 in mass, and particularly at low energies, where any specific mass effects would be most pronounced [1,2,22,25]. Though studies with energy-degraded muon beams in the range ~8–80 keV in metal targets [55] indicated that velocity scaling holds well in comparison with the equivalent proton data, both theory [22] and more recent experimental results to even lower muon energies (0.5 to 30 keV) [1] show that at these energies proton stopping powers could be enhanced, at least in metals, by a few percent. Since density effects can be significant in stopping powers [56–58], it is important to also be able to compare muon and proton stopping powers in low density gases, providing partial motivation for the present study, which, to our knowledge, is the first of its kind.

The classic stopping-power formula of Eq. (1) is for a single element or homopolar diatomic, but needs to be modified for a molecular compound or mixture of k different kinds of atoms $i=1,2,3,\ldots,k$, and given by

$$-\left(\frac{dE}{dx}\right)=\frac{4\pi e^4 z_p^2}{m_e v^2}\sum_{i=1}^{k}\ln\left(\frac{2m_e v^2}{I_i}\right)^{z_i n_i}=\frac{4\pi e^4 z_p^2 Z_T n}{m_e v^2}\ln\left(\frac{2m_e v^2}{I_T}\right) \tag{3}$$

with excitation parameters I_i and atomic numbers Z_i, and where n_j is the number density of *atoms* of type i, n is the density of target *molecules*, and Z_T represents the total charge defined by

$$Z_T n = Z_1 n_1 + Z_2 n_2 + \cdots + Z_k n_k = \sum_{i=1}^{k} Z_i n_i, \tag{4}$$

giving the average number of electrons per molecule. The average excitation energy is correspondingly defined by

$$\ln I_T = \frac{Z_1 n_1}{Z_T n}\ln I_1 + \frac{Z_2 n_2}{Z_T n}\ln I_2 + \cdots + \frac{Z_k n_k}{Z_T n}\ln I_k = \sum_{i=1}^{k}\frac{Z_i n_i}{Z_T n}\ln I_i. \tag{5}$$

The extensions of the Bethe-Bloch formula to a molecule or mixture, shown in Eqs. (4) and (5), are known historically as "Bragg's additivity rules" [50,53,54,59,60] and which have been applied recently in polymers [45,61]. Their principal assumption is that physical state and chemical bonding are irrelevant, so each atom in a mixture or molecule can be treated independently. Deviations from Bragg's rule can be appreciable though, $\gtrsim$20% [54,60,61], particularly at low energies, not only due to its neglect of shell corrections but also near the Bragg peak in the stopping power, where charge exchange becomes important [54,62].

An important and unique aspect of the present study is the *time* spent in the Bethe-Bloch regime, denoted by t_{BB}^{+}, during which the particle slows from an initial energy E_i (velocity v_i) down to some final energy E_f (velocity v_f), at which the first Mu or H formation takes place. For a continuous energy loss, $dE/dt=(dE/dx)(dx/dt)$, and hence this time, for a positive muon (or proton), can be expressed in terms of the stopping power of Eq. (1) in the BB regime, $(dE/dx)_+$, by

$$t_{BB}^{+}(E_i,E_f)=m\int_{v_i}^{v_f}\frac{dv}{(dE/dx)_+}=\int_{E_i}^{E_f}\frac{dE}{v(dE/dx)_+}, \tag{6}$$

where E_f is later interpreted as $\langle E_{CE}\rangle$, the *average* energy at which Mu (H) first forms.

B. Cyclic charge exchange

In the Bethe-Bloch regime, the velocity of the projectile (v) is much larger than that of electrons (v_e) in the moderator atoms. At some energy E_{CE}, v and v_e become roughly comparable, and the muon (proton) captures an electron from the moderator, staying in this neutral charge state for some time, until its bound electron is lost in a subsequent collision, forming again a positive species at some lower energy and thus initiating a series of CE cycles. An early discussion of the charge exchange of protons in gases was the work of Allison [38] and this treatment was utilized in the first detailed experimental work on μ^+ charge exchange in low pressure gases by Fleming *et al.* [16,17], with additional data of this nature since obtained over a range of pressures and conditions [10,11,18,47,48,63].

Once a Mu atom is formed at some energy E_j (velocity v_j), the probability that it does *not* undergo any electron loss collision down to energy E (velocity v) is given by the survival probability function [13,26–28]

$$S_L(E_j,E)=\exp[-N_L(E_j,E)], \tag{7}$$

where the collision number $N_L(E_j,E)$ is expressed in terms of the electron *loss* cross section $\sigma_L(E)$ by

$$N_L(E_j,E)=\int_0^t n v\sigma_L dt=\int_{E_j}^{E}\frac{n_v\sigma_L(E)}{(dE/dx)_0}dE=m\int_{v_j}^{v}\frac{nv\sigma_L(v)}{(dE/dx)_0}dv. \tag{8}$$

Here, the quantity $(dE/dx)_0$ is the stopping power for the *neutral* atom (Mu or H), which can be expressed in terms of the cross sections of the atomic processes contributing to its slowing down [13,26],

$$\left(\frac{dE}{dx}\right)_0 = n \ln f_0(E)\left[E + \frac{I_0(E)}{1-f_0(E)}\right]\sigma_0(E). \tag{9}$$

The quantities $f_0(E)$ and $I_0(E)$ are elastic and inelastic (ionization, excitation, …) energy-loss parameters, averaged over the collisional scattering-angle dependences and $\sigma_0(E)$ is the total collision cross section of the neutral particle but *excluding* the electron-loss process, since this produces the positive particle and changes the species identity [26]; i.e., $\sigma_0(E)=\sigma_{0E}(E)+\sigma_{0I}(E)+\sigma_{0X}(E)+\cdots$.

The residence time in the charge state s, during the jth charge exchange cycle, is denoted t_j^s, while E_j^s is the energy at which the species s is formed. Thus, if Mu is produced at E_j^0 during the jth cycle, the mean energy for the next electron-loss collision $\langle E\rangle$ can be obtained from the condition $N_L(E_i^0,\langle E\rangle)=1$ in accordance with the usual definition of the mean free path and time [26]. Using this $\langle E\rangle$, the mean residence time in muonium during the jth charge-exchange cycle can be written in a form similar to Eq. (6), as

$$t_j^0(E_j^0,\langle E\rangle) = \int_{E_j^0}^{\langle E\rangle} \frac{dE}{v(dE/dx)_0} = \int_{E_j^0}^{E_j^0-\langle e_j^0\rangle} \frac{dE}{v(dE/dx)_0}, \tag{10}$$

where $\langle e_j^0\rangle$ is the energy loss during t_j^0.

Similarly, the survival function of the charged species (muon or proton) to electron capture can be denoted by a change in subscripts, L→C and 0→+, in Eq. (8), giving accordingly, the mean residence time in the positive muon charge state during the jth charge-exchange cycle as

$$t_j^+(E_j^+,\langle E\rangle) = \int_{E_j^+}^{\langle E\rangle} \frac{dE}{v(dE/dx)_+} = \int_{E_j^+}^{E_j^+-\langle e_j^+\rangle} \frac{dE}{v(dE/dx)_+}, \tag{11}$$

which has the same form as Eq. (10) for the neutral species.

C. Final thermalization and muonium observation

After many cycles of charge exchange collisions, the incident (μ^+) particle emerges from the CE regime either as a neutral Mu atom or a positive muon, depending on the threshold energies E_C^{TH} and E_L^{th} for electron capture and loss processes at the *end* of the cyclic charge exchange regime [26]. The threshold for electron loss is $E_L^{th}\approx 13.6$ eV, the same as the ionization energy (E_{ion}) of Mu (or H) itself, but E_C^{th} depends also on this energy for the moderator ($E_C^{th}\approx E_{ion}-13.6\approx 2$ eV for Mu-H in Ar). The fraction of muons thermalized as muonium and observed experimentally (Mu fraction) depends on the competition between charge exchange and moderation processes: how fast Mu, produced above E_L^{th}, reaches E_L^{th} before an electron-loss collision takes place, and how slowly a positive muon slows down so that one more electron capture is possible before E_C^{th} is reached. Both of these effects determine the energy at which the *last* Mu atom is produced, first estimated to be about 30 eV in Ar [16] and later calculated more accurately, giving ≈10 eV [28]. As introduced above and discussed below in some detail, the SD time reported herein is from an initial energy E_i down to the energy at which Mu is formed for the last time, ending the last charge-exchange cycle.

Once formed, and *after* cyclic CE, at energies ≈10 eV, the Mu atom thermalizes in the gas (to kT) by elastic and inelastic collisions, but the bare μ^+ can still form Mu in moderators with low enough threshold energies, E_C^{th} (the case in most gases). Thus, the Mu fractions measured at low pressures of the inert gases He, Ne, Ar, Kr, Xe, and N_2 are 0.0, 0.0, 0.75, 1.0, 1.0, and 0.85, respectively [11,16,48,63], with uncertainties typically ±0.04. (There is no Mu seen in He or Ne because E_C^{th} is too high.) The diamagnetic muon fraction seen in these gases is exclusively in the form of molecular ions (e.g., $HeMu^+$), formed promptly [11] by *muon* addition at energies ~1 eV, well below that of the last Mu formation [17,18].

In contrast to noble or inert molecular gases, in most molecular gases, energetic hydrogen atoms (Mu^*, H^*, or T^*) emerging from the CE regime may undergo epithermal or "hot atom" chemical reactions in the energy range ~10 eV to 0.5 eV, reducing the amount of Mu observed [13,14,34,48]. The probability that Mu survives from some initial energy E_i, in the thermalization regime, down to thermal energy $E_T=\frac{3}{2}kT$, i.e., that Mu does *not* undergo a reactive (hot atom) collision, can be expressed by a form analogous to Eq. (7), but in terms of the *reaction* cross section, $\sigma_R(E)$, for forming a stable diamagnetic product. This in turn can be utilized to express the hot atom reaction "yield" as $Y_R(E_i,E_T)=1-S_R(E_i,E_T)$, which has been calculated explicitly for the Mu^*+H_2 and T^*+H_2 reactions, in which both elastic and inelastic moderation was explicitly accounted for by quasiclassical trajectory (QCT) calculations [13], giving good agreement with experiment [13,64]. Since similar H-abstraction reactions can also give rise to *thermal* reaction rates [31,32,65], knowledge of the final thermalization time is crucial for clarifying this distinction, and is an important part of the present paper (Sec. VII).

III. PRINCIPLE OF THE MEASUREMENT

An external magnetic field (z direction) is applied transverse to the muon spin. The muon polarization is then conveniently represented as a complex quantity, where the real and imaginary parts correspond to the x and y components, respectively, and the initial muon polarization is taken along the x axis. The time evolution of the spin of the bare positive muon is given by

$$G_+(t) = \exp(-i\omega_\mu t), \tag{12}$$

where $\omega_\mu=2\pi\nu_\mu=\gamma_\mu B$, from which it follows that the muon Larmor precession frequency is $\nu_\mu=0.01355$ MHz/G×B, where B is the field in gauss. Here, the muon spin precesses clockwise in the x-y plane, when viewed from the positive z direction.

When the positive muon captures an electron to form muonium, the system is described by the well-known (Breit-Rabi) Hamiltonian, consisting of two Zeeman terms for the muon and the electron and a hyperfine coupling term $\nu_0\mathbf{S}_\mu\cdot\mathbf{S}_e$, where $\nu_0=\omega_0/2\pi=4463$ MHz is the isotropic

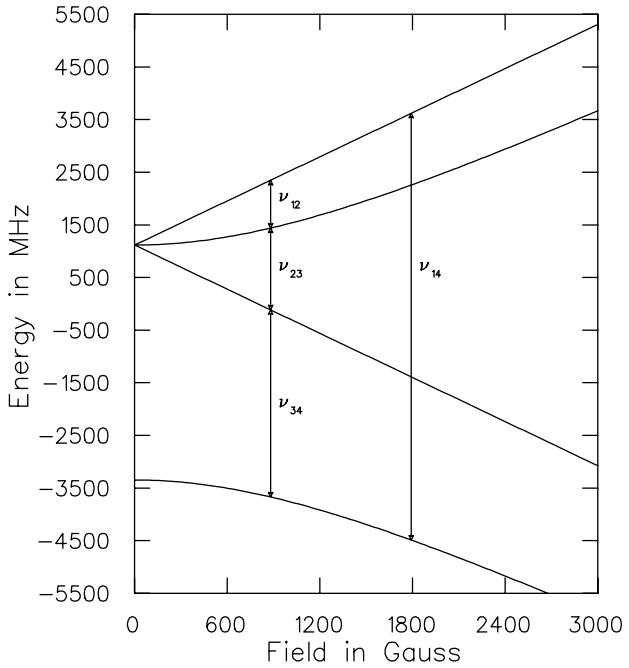

FIG. 1. Breit-Rabi energy level diagram of muonium. At $B=0$ the triplet and singlet states are separated by $\nu_0=4463$ MHz. Equation (13) gives the energy differences manifest as the precession frequencies indicated in the figure, ω_{12}, ω_{23}, ω_{14}, and ω_{34} defined by $\omega_{jk}=2\pi(\nu_j-\nu_k)$. In the weak-field region of interest ($B<10$ G), ω_{12} and ω_{23} are degenerate, giving rise to the coherent precession of triplet muonium.

$\mu-e$ hyperfine coupling constant [35,66]. The eigenenergies vs magnetic field strength are shown in Fig. 1. The muon spin polarization in a transverse field (TF) is shared among the four distinct precessing components indicated in the figure, so its time evolution is more complicated than for the bare muon [14,15,28]

$$G_0(t)=\tfrac{1}{2}c^2[e^{i\omega_{12}t}+e^{-i\omega_{34}t}]+\tfrac{1}{2}s^2[e^{i\omega_{23}t}+e^{-i\omega_{14}t}], \quad (13)$$

where $\hbar\omega_{ik}=\hbar(\omega_i-\omega_k)$ is the energy difference between the ith and kth states of the Breit-Rabi diagram (Fig. 1) and c^2 and s^2 relate to the applied field, expressed in terms of $B/B_0(B_0=1585$ G for Mu) by

$$c^2=\tfrac{1}{2}\left[1+(B/B_0)/\sqrt{(B/B_0)^2+1}\right], \quad (14)$$

$$s^2=\tfrac{1}{2}\left[1-(B/B_0)/\sqrt{(B/B_0)^2+1}\right]. \quad (15)$$

Now, let $\{t_j^s\}=t_1^0t_1^+t_2^0t_2^+\ldots t_N^0t_N^+$ be a sequence of residence times in the charge state s, during the jth charge-exchange cycle, up to the *last* muonium (Mu) formation. Thus the combined SD time introduced above, through the BB and CE regimes, from Eqs. (6), (10), and (11), has the form

$$t_{\mathrm{SD}}=t_{\mathrm{BB}}^+ + \sum_{j=1}^{N}(t_j^0+t_j^+)=t_{\mathrm{BB}}^+ + t_{\mathrm{CE}}, \quad (16)$$

where t_{CE} is the time spent in the CE regime alone. The complex polarization of the muon spin in muonium *after* the final muonium formation, i.e., at time t later than t_{SD}, is given by [28,36]

$$P(t)=G_0(t-t_{\mathrm{SD}})P(t_{\mathrm{SD}})=G_0(t-t_{\mathrm{SD}})\exp(-i\omega_\mu t^+)\prod_{j=1}^{N}G_0(t_j^0), \quad (17)$$

where $t^+=t_{\mathrm{BB}}^+ + \Sigma_{j=1}^N t_j^+$ is the total time in the *positive* muon state.

It is instructive to investigate $G_0(t)$ more closely in two different time domains, $t\gg 0.224$ ns and $t\ll 0.224$ ns, where $1/\nu_0=0.224$ ns is the Mu hyperfine period. The quantity t in $G_0(t-t_{\mathrm{SD}})$ is the *observation* time, which is on the order of microseconds, the time regime of the first domain. In this domain, since the conventional TF-μSR technique employed here has a typical time resolution of a few ns, $e^{i\omega_{14}t}$ and $e^{-i\omega_{34}t}$ in Eq. (13), both of which oscillate at a frequency comparable to ω_0, are not observed. Furthermore, in the low fields of interest ($B<10$ G), where $c^2=s^2=1/2$, the angular frequencies ω_{12} and ω_{23} are equal ($\nu_{12}=\nu_{23}$ in Fig. 1), giving, accordingly, the Larmor precession frequency of "triplet" muonium, $\nu_{\mathrm{Mu}}=\omega_{\mathrm{Mu}}/2\pi=1.39$ MHz/G$\times B$, largely determined by the dominant magnetic moment of the electron. It follows then that the quantity $G_0(t-t_{\mathrm{SD}})$ detected in a weak-TF μSR experiment can be simplified to

$$G_0(t-t_{\mathrm{SD}})=\tfrac{1}{2}\exp[i\omega_{\mathrm{Mu}}(t-t_{\mathrm{SD}})], \quad (18)$$

where the factor 1/2 accounts for the fact that only the triplet ensemble is observable in such fields. Because of the sign of the electron gyromagnetic ratio, the muon spin in Mu precesses in the opposite direction to the free muon spin precession given by Eq. (12).

Substituting Eq. (18) into Eq. (17), gives, for the weak-field muon polarization in muonium,

$$P(t)=\tfrac{1}{2}\exp[i\omega_{\mathrm{Mu}}(t-t_{\mathrm{SD}})]\exp(-i\omega_\mu t^+)\prod_{j=1}^{N}G_0(t_j^0), \quad (19)$$

where $G_0(t_j^0)$ represents the time evolution of the muon spin during the jth muonium residence time of the charge exchange regime. Residence times t_j^0 in the Mu charge state in gases like Ar and N_2 at ~ 1 atm pressure are much shorter than the hyperfine period, 0.224 ns (see also Ref. [16]), i.e., $\omega t_j^0\ll 1$, for all ω_{ik} in Eq. (13). Thus $G_0(t)$ can be simplified to

$$G_0(t)\approx 1+\frac{c^2}{2}i(\omega_{12}-\omega_{34})t+\frac{s^2}{2}i(\omega_{23}+\omega_{14})t$$
$$=1-i\omega_\mu t\approx\exp(-i\omega_\mu t). \quad (20)$$

It is worth noting that if t_j^0 were actually comparable to 0.224 ns, this would completely depolarize the muon spin, resulting in $P(t)=0$. Thus, as long as Mu precession, $P(t)$, can be observed, the condition $t_j^0\ll 0.224$ ns is satisfied.

Equation (20) expresses the important result that, for very short Mu residence times, the muon spin in Mu precesses as if the muon were completely free. In other words, before the muon spin in Mu starts precessing counterclockwise with frequency ω_{Mu}, the muon spin always moves momentarily

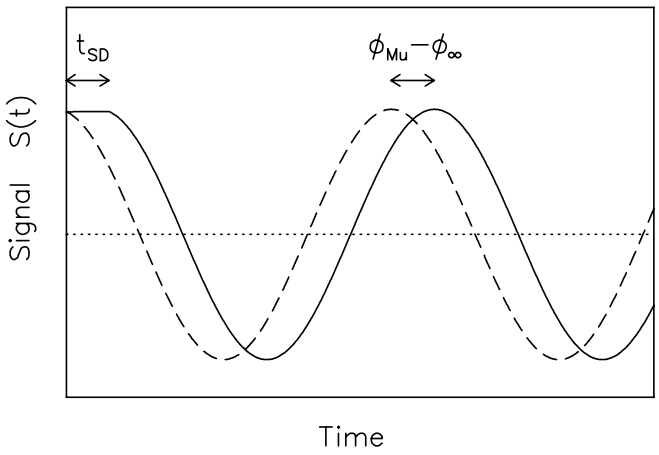

FIG. 2. Simulated precession signal (dashed curve) for Mu with zero slowing down time and initial phase ϕ_{∞}, and a more normal signal for Mu (solid) with slowing down time t_{SD}, during which the Mu nuclear spin precesses slowly backwards, giving an apparent initial phase $\phi_{Mu} \neq \phi_{\infty}$.

clockwise (*quantum backswing*) [28,29,66]. If each muonium residence time during charge exchange is much shorter than the hyperfine period, the product $\Pi_{j=1}^{N} G_0(t_j^0)$ in Eq. (19) can be simplified to $\exp(-\omega_\mu t^0)$, where $t^0=\Sigma_{j=1}^{N} t_j^0$ is the total time in the muonium charge state. Therefore, the muon polarization *after the last muonium formation* can be expressed by

$$P(t) = \tfrac{1}{2} \exp[-i(\omega_{Mu} + \omega_\mu)t_{SD}] \ \exp[i\omega_{Mu} t]. \qquad (21)$$

It can be seen from Eq. (21) that the precession of triplet muonium acquires an initial phase proportional to the slowing-down time in the BB and CE regimes [Eq. (16)]. This is the essence of the present technique.

Figure 2 illustrates these phases generically. The dashed sinusoid is the expected weak-field precession of Mu with *zero* slowing-down time ($t_{SD}=0$) and initial phase ϕ_{∞}, which depends on the initial muon spin direction but not on the type of target gas (though the hypothetical gas would be infinitely dense). The solid curve is the precession signal for Mu at some nominal pressure, having a slowing-down time t_{SD}, and during this time, the (reverse) muon precession is too slow to be visible in the diagram. After the final formation of muonium, when normal muonium precession sets in, the signal has acquired a phase offset of $\phi_{Mu}-\phi_{\infty}=(\omega_{Mu}+\omega_\mu)t_{SD}$, proportional to the slowing down time.

At the low (few atm) pressures of interest, slowing down times are expected to be inversely proportional to the gas density (n), so, from Eq. (21), it follows that the phase at a given n can be expressed as

$$\phi_{Mu}(n) = \phi_{\infty} - (\omega_{Mu} + \omega_\mu)\tau_{SD}\, n_0/n \qquad (22)$$

where τ_{SD} is a normalized or "characteristic" slowing-down time, defined as the value of t_{SD} at the density, n_0, of the gas at standard conditions of 1 atm and 300 K; i.e., $\tau_{SD} \equiv t_{SD} n/n_0$. By measuring the initial phases of Mu precession at several gas pressures, one can determine this SD time, τ_{SD}. It is important to emphasize that this is the μ^+ slowing-down time from an initial energy ~2 MeV, entering the BB regime, *to the end of the last Mu-formation cycle*, which is about 10 eV in the case of Ar [28]. It is a completely separate question what the time is for the Mu atom (or μ^+) to thermalize further, in its final regime, during which there is no further *cyclic* charge exchange. This regime is addressed further below.

IV. EXPERIMENT

The μSR technique relies on the fact that positive muons are produced 100% spin polarized from pion (π^+) decay, and then in turn they themselves decay ($\mu^+ \rightarrow e^+ + \bar{\nu}_e + \bar{\nu}_\mu$) to emit positrons *preferentially* along the muon spin direction, independent of environment, as a consequence of parity violation in the weak interaction [14,15]. Detection of these decay positrons allows the time evolution of the muon spin to be monitored, in a given environment. The SD-time measurements reported here involved measuring the initial phase of Mu spin precession in various gases, utilizing the principle described above.

An aluminum target vessel 50 cm in diameter and 100 cm long was placed in the middle of a set of large Helmholtz coils (150 cm diameter), which provided a homogeneous field set at low B values in the range ~5–10 G, parallel to the muon beam direction. Additional pairs of correction coils were used to eliminate any transverse component of the fringe cyclotron field. Pressures of the different gases and gas mixtures used were in the range ~0.2 to 3.5 atm and measured with a Baratron capacitance manometer. This range is limited by the strength of the muon-entrance window (0.13 mm Kapton) of the target vessel at high pressure and loss of measurable signal amplitude at low pressure. Gas densities were calculated from the measured pressures and ambient temperatures using the ideal gas law. Incoming muons were detected by a plastic scintillator counter of 0.25 mm thickness placed in front of the beam entrance window. Decay positrons were detected by two sets of positron detectors, each consisting of two 30 cm × 30 cm plastic scintillators, placed above and below the target vessel, 50 cm and 60 cm from the center of the coils, respectively.

Our experiment utilized "surface muons," arising from the decay of pions at rest, on the M15 and M20 beamlines at the TRIUMF cyclotron [67]. Surface muons have a nominal energy of 4.1 MeV, but there is a distribution of particle energies produced, and some of the initial energy is also lost in traversing beam line windows and the muon scintillator. The resultant muon energy was then measured by a surface barrier detector of 2 mm thickness (enough to stop 4 MeV muons) positioned inside the evacuated target vessel (and later removed). This detector was calibrated by α decay from ^{146}Gd and ^{241}Am at kinetic energies of 3.18 and 5.48 MeV, respectively. Different beam tunes were used to deliver muons with initial energies measured *in* the target vessel of E_i=1.1±0.3, 1.6±0.3, 1.8±0.4, 2.2±0.3, 2.4±0.4, and 2.8±0.3 MeV, where the quoted uncertainties are half the width of the measured energy distribution. It can be noted that the present technique is not amenable to measurements in dense media at all, or in gases at initial energies much

lower than ~1 MeV, the latter due to constraints on both muon flux and penetrating power (through thin windows and the muon counter).

A Wien filter [67] installed on the beamline rotated the muon spin by 90° from its natural longitudinal orientation to point upwards, transverse to both the beam and the applied magnetic field. Transverse muon polarizations were important in this experiment for avoiding a type of systematic error: with the muon (μ^+) spin pointing vertically and the field applied along the beam direction, the spin precesses in a plane perpendicular to the beam, ensuring that the initial muonium phase is insensitive to the changing stopping location of muons as the target pressure is varied.

V. DATA ANALYSIS AND RESULTS

In the basic μSR experiment, an incoming muon is detected by the muon counter, starting a time-to-digital converter ("clock"), which is subsequently stopped by the detection of a decay positron, and such decay events are sorted by time to form a histogram, $N(t)$. These time histograms, from each separate pairs of detectors, were fit to a standard μSR fitting function [9,14,15]

$$N(t) = N_b + N \exp(-t/\tau_\mu)[1 + A(t)], \tag{23}$$

where N_b is a time-independent background, N is a normalization factor, τ_μ is the muon life time (2.2 μs), and $A(t)$ is the μSR signal of interest. For a weak transverse field ($B \lesssim 10$ G), this is given by

$$A(t) = A_{Mu} \exp(-\lambda_{Mu} t) \cos(\omega_{Mu} t + \phi_{Mu}) + A_D \cos(\omega_D t - \phi_D). \tag{24}$$

The quantities ϕ_{Mu} and ϕ_D are the initial phases of the muonium and diamagnetic muon signals, respectively, A_{Mu} and A_D are the corresponding initial amplitudes, and λ_{Mu} is the relaxation rate of muonium. The first term of Eq. (24) has its origin in Eq. (18), for observation times $t \gg t_{SD}$, while the second term comes from Eq. (12). For all practical purposes, $\omega_D = \omega_\mu$, for muons in any diamagnetic environment, since small chemical shifts cannot be resolved. In the absence of chemical and spin exchange reactions, as in the present study, λ_{Mu} is determined primarily by the inhomogeneity of the applied field over the muon stopping distribution. The quantity of primary interest in this work is ϕ_{Mu}, which varies linearly with the slowing-down time, as defined by Eq. (22). The beginning of the time histogram (so-called *time zero*, t_0) is determined from the inflection point of the signal's initial rise, from N_b to approximately $N+N_b$, within $\approx$2 ns. This uncertainty in t_0, which introduces an uncertainty in the initial phase, will not affect the slope of a ϕ_{Mu} vs $1/n$ plot.

At the highest gas pressure used in this experiment (3.5 atm), muons stopped near the upstream edge of the positron detectors, depending on E_i. As the target pressure was decreased, the muon range increased and the stopping region moved downstream, but if the gas pressure were to get too low, muons would stop far downstream from the positron counters, leading to an artificially long slowing-down time, due to delay of the signal by the long transit time of decay positrons to the detectors. Such variations would cause a deviation from the expected linearity between the phase and $1/n$ in Eq. (22), so an experimental requirement was that the muons must stop *between* the positron detectors, which is the central region of the magnet. Knowing the field distribution of the Helmholtz coils, one can use ω_{Mu} and λ_{Mu} as indicators of where muons are stopping in the target vessel. Note that constant transit times within the central volume will contribute to ϕ_∞ of Eq. (22) but not to the slope of a ϕ_{Mu} vs $1/n$ plot.

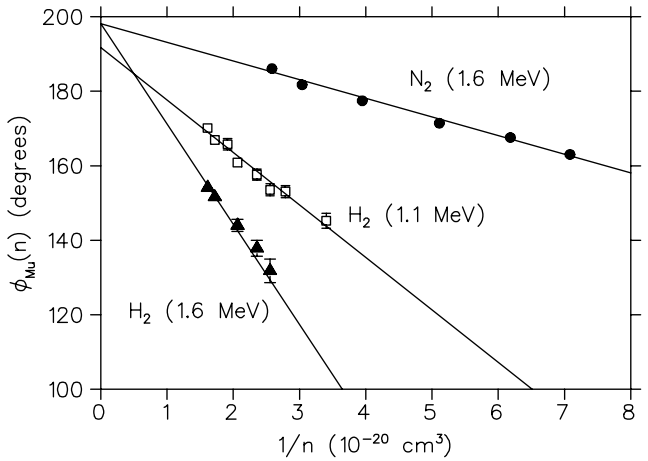

FIG. 3. Muonium phase in the downward direction plotted vs reciprocal density for N_2, with an initial muon energy of 1.6 MeV (solid circles), and for H_2 with muon energies of 1.1 and 1.6 MeV (squares and solid triangles, respectively). The straight lines are fits to Eq. (22), constrained to have the same intercept ϕ_∞ for the same energy, whose slopes give the characteristic muon slowing time τ_{SD}. It is clear that the μ^+ has a much longer slowing time in H_2 than in N_2, and that the slowing down time is longer for higher-energy muons.

For a given gas, base measurements were done in a decreasing order of pressure until A_{Mu} became too low, or a deviation from the desired linearity of ϕ_{Mu} vs $1/n$ given by Eq. (22) was observed, or until ω_{Mu} or λ_{Mu} indicated the stopping region of muons was far from the center of the coils. The initial phases in two opposing directions (up and down) were determined for a range of pressures of pure Ar, N_2, and H_2, and mixtures of He-Ar, Ne-Ar, He-H_2, CF_4-Ar, and SF_6-H_2. Figure 3 shows a plot of ϕ_{Mu} recorded by the downward detector (opposite to the initial muon spin direction) vs $1/n$ for N_2 and H_2, and initial muon energies of 1.6 and 1.1 MeV. Similarly, Fig. 4 shows the linear variation of ϕ_{Mu} with $1/n$ of pure Ar and Ar mixtures, for an initial muon energy $E_i = 1.8$ MeV, but as recorded in the upward detector. The slopes are of prime importance since these give the characteristic (1 atm) slowing-down times of interest, τ_{SD}.

The initial phases for all pressures of all gases measured at a particular initial energy were simultaneously (globally) fit to Eq. (22), to give separate values of τ_{SD} for each gas or gas mixture, along with two shared values of ϕ_∞—one for each detector direction, up or down. Noteworthy in Fig. 3 is that the fits for 1.6 MeV muons converge to the same intercept (ϕ_∞) for N_2 and H_2, but 1.1 MeV muons in H_2 give a different intercept. At both energies, the H_2 lines are steeper

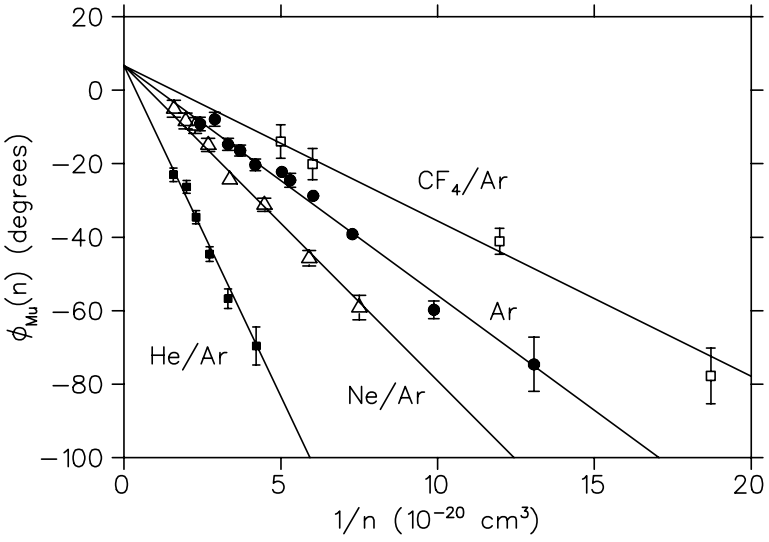

FIG. 4. Muonium phases measured in the upper detector for pure Ar (solid circles) and Ar mixtures: He-Ar (25% Ar, solid squares), Ne-Ar (37% Ar, triangles), and CF_4-Ar (67% Ar, squares); all with muon energy E_i=1.8 MeV. The straight lines are fits constrained to give the same ϕ_∞ (intercept) but individual slopes, which give τ_{SD} directly.

than for N_2, indicating a greater τ_{SD} for H_2. The 1.6 MeV H_2 line is also steeper than for 1.1 MeV, since it takes a longer time to slow down from a higher energy, seen also from the entries in Tables I and II below.

The gas mixtures studied were He-H_2 (50% H_2), SF_6-H_2 (97% H_2), He-Ar (25% Ar), Ne-Ar (37% Ar), and CF_4-Ar (67% Ar), with the intent in part of testing the (Bragg) additivity rule of Eqs. (4) and (5), as well as to examine energy moderation effects in the SD process. More specifically, elastic moderation efficiencies were compared by mixing different-massed inert gases with Ar (the series Ar, He-Ar, and Ne-Ar) and with H_2 (H_2 and He-H_2); the effects of chemical binding and inelastic moderation on the slowing-down time were examined by comparing H_2 with He-H_2, CF_4-H_2, and SF_6-H_2, the molecular gases SF_6 and CF_4 having many internal degrees of freedom. An additional, pragmatic, motivation in the cases of He and Ne, was that a gas with a lower ionization potential was needed for any Mu to be formed [14,16].

TABLE I. Muon slowing down times [τ_{SD} (ns)] from the initial muon energy (E_i) to that of the last muonium formation (≈10 eV) in pure gases at 1 atm and 300 μK.

E_i (MeV)	H_2	D_2	N_2	Ar[a]
2.8(0.3)[b]			14.3(0.6)	13.3(0.5)
2.4(0.4)			10.4(0.4)	10.4(0.6)
2.2(0.3)				9.3(0.6)
1.8(0.4)			7.0(0.2)	6.8(0.2)
1.6(0.3)	34.2(0.7)		6.5(0.2)	6.4(0.2)
1.1(0.3)	18.1(1.4)			
≈0.9[c]	10.9(0.8)	10.3(0.8)		

[a]Most of the Ar entries were reported earlier, in a demonstration of the technique [28], with the exception of the entry at 2.2 MeV, which was measured in the present study, along with all the other entries in the table.

[b]Initial muon energies and widths of the energy distribution measured with a surface barrier detector. Uncertainties in the central (mean) energy are expected to be less than the widths and are estimated to be ≈0.1 MeV. Errors given for the SD times are only from the least-squares fits (Figs. 3 and 4).

[c]Muon energy was not measured but determined from beamline magnet settings, with an uncertainty also estimated as ≈0.1 MeV.

Table I gives the muon slowing-down times, τ_{SD} (in ns), measured in pure H_2, D_2, N_2, and Ar, at various initial energies, while Table II gives these times for the mixtures listed above. The energy errors given in Tables I and II are the measured widths given earlier, for the distribution of muon energies, as measured by the surface barrier detector. The errors in the values of the central (mean) energies, affecting the values of τ_{SD}, are believed to be much less than the widths, and are estimated to be uncertain by ≈0.1 MeV. Though this is a comparable percent error to those quoted from the determination of τ_{SD} from the least-squares ("minuit") fits of the slopes (Figs. 3 and 4), it is also not well determined, so only the latter errors are shown for the SD times in Tables I and II. On the other hand, any uncertainty in the energy measurement would apply to all gases measured at that energy, and so could generate some systematic error in τ_{SD}. There is some evidence for this in a comparison of N_2 and Ar measured at 1.6 and 1.8 MeV where, for both gases, the slowing times are perhaps closer than the energies would suggest.

Figure 5 shows the pressure dependence of the muonium phase in H_2 and D_2, from data taken in previous experiments [31,64] using the same target vessel as in the current measurements. In this case though the initial muon energy was not measured directly, but rather an estimate of E_i was made from a comparison of muon momenta from the recorded

TABLE II. Muon slowing down times (τ_{SD}/ns) for gas mixtures at 1 atm and 300 K.

E_i(MeV)	He-H_2 (50% H_2)	SF_6-H_2 (97% H_2)	He-Ar (25% Ar)	Ne-Ar (37% Ar)	CF_4-Ar (67% Ar)
1.8(0.4)			19.6(0.6)	9.3(0.3)	4.6(0.3)
1.6(0.3)	35.9(0.9)	20.2(1.3)			
1.1(0.3)	18.4(1.9)	9.4(2.3)			

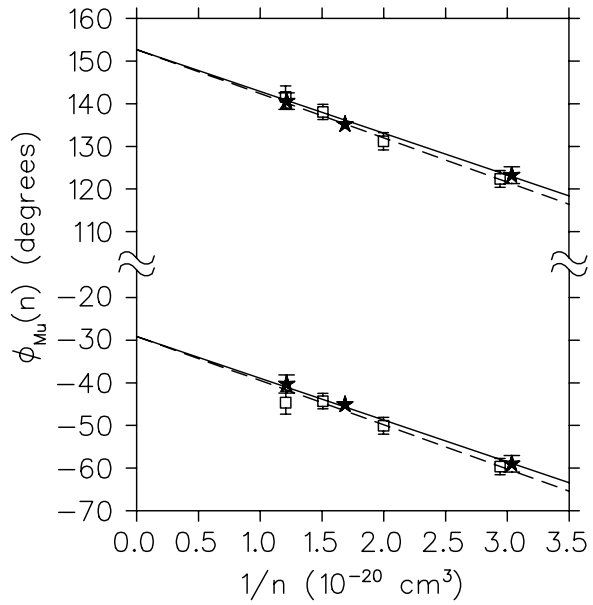

FIG. 5. A plot of Mu phase for H_2 (squares and dashed lines) and D_2 (stars; solid) as in Figs. 3 and 4, but with the data from both the upward and downward detectors plotted (lower and upper data, respectively). The initial μ^+ energy was approximately 0.9 MeV, although it was not measured directly.

beam line settings, giving an energy in the target $E_i \approx 0.9$ MeV, which we also estimate as having an uncertainty of 0.1 MeV. Though the energy could even be more uncertain here, this does not affect the comparisons between H_2 and D_2 shown, and hence their slopes, τ_{SD}, which is the central point of the data plotted in Fig. 5.

VI. DISCUSSION

A. Qualitative aspects of measured SD times, τ_{SD}

The central experimental results of the present study are the slowing-down times, τ_{SD}, reported in Tables I and II. These are the times the muon spends in the Bethe-Bloch *and* charge-exchange regimes, from ~2 MeV to 10 eV, as defined by $t_{SD}=t_{BB}^{+}+t_{CE}$ [Eq. (16)]. It will be shown below that t_{CE} is much less than t_{BB}^{+}, established earlier in Ref. [16] as well, so that, effectively, $t_{SD} \approx t_{BB}^{+}$. The measured SD times show the expected dependence on initial energy mentioned above, higher energies (E_i) giving longer times. Since N_2 has a smaller effective excitation energy, I, than Ar[52] but a smaller total charge, Z_T, these two effects tend to be compensating in Eq. (1), leading to similar SD times. In contrast, H_2, with the smallest charge, has a significantly slower rate of energy loss and correspondingly a longer SD time. Kinematics and energy-moderation cross sections also play a role here. In this regard, it is interesting to note from Table I that τ_{SD} in H_2 and D_2 are the same (within errors), suggesting that *inelastic* scattering, here between widely spaced rovibrational levels in molecular gases, plays a more important role than elastic scattering in the energy moderation processes, in the BB and CE regimes. On the other hand, the similar SD times for N_2 and Ar, both much less than in H_2 (D_2), also shows that elastic energy moderation is still important in all gases.

The role of total charge as well as elastic and inelastic energy moderation effects is reflected as well in the SD times for the mixtures shown in Table II. Thus for $E_i=1.8$ MeV, the Ne-Ar and particularly He-Ar mixtures, with reduced total charges, have longer SD times than Ar itself, whereas that for CF_4-Ar is significantly shorter due to both the inelastic (rovibrational) contributions from the molecular component, and a somewhat higher total charge. Similarly, while a 50% mixture of He-H_2 has the same SD time (and the same Z_T) as pure H_2, only 3% of SF_6 in H_2 cuts this time in half. It is also worth noting here that, e.g., the addition of He to Ar should raise the average energy for the last Mu formation significantly, from about 10 eV in pure Ar [28] to possibly tens of eV in He-Ar [26], and yet this has little or no effect on the measured SD time. In like manner, recent results showing charge exchange cross sections for H^+ being different by as much as 50% between H_2 and D_2 [68] at sub-keV proton energies, or at equivalent ~20 eV μ^+ energies, near the end of the CE regime, do not impact on the equal SD times noted above. Both of these results are consistent with the previous statement that this time is due almost exclusively to energy loss in the BB regime.

B. The muon stopping powers, $S(E)$

It has been shown elsewhere that the time spent in the CE regime, t_{CE} does not depend on the initial energy (E_i) as long as $E_i \gg E_{CE}$, the energy of the *first* Mu formation (see below) [28], so that the muon stopping power at E_i can be found by differentiating Eq. (6), giving for the energy loss,

$$\left(\frac{dE}{dx}\right)_{E_i} = -\frac{1}{v_i}\frac{dE_i}{dt_{SD}}, \tag{25}$$

leading to

$$S(E) = -\frac{1}{n}\frac{dE}{dx} = \left(n_0 v_i \frac{d\tau_{SD}}{dE_i}\right)^{-1} \tag{26}$$

for the μ^+ stopping power per molecule, where n_0 is again the gas density at 300 K and 1 atm pressure.

Both N_2 and Ar were studied over a sufficiently wide range of initial energies ($E_i=1.6$ to 2.8 MeV, in Table I) to determine the slope $d\tau_{SD}/dE_i$ well, and hence their stopping powers from Eq. (26). Pure H_2 and an H_2-He mixture were also studied at two (measured) energies, allowing a determination of their μ^+ stopping powers. We have used two methods to calculate $d\tau_{SD}/dE_i$ from the data, as illustrated in Fig. 6, which plots τ_{SD} vs E_i for Ar [Fig. 6(a)] and N_2 [Fig. 6(b)]. Figure 7 plots the stopping power, $S(E)$, derived from both methods, compared with the corresponding proton stopping [Fig. 6(a)] powers [39–41,69].

The first method was to determine $d\tau_{SD}/dE_i$ over the discrete intervals between data points. However, there would be too much uncertainty in the slope if taken between closely spaced points, so some pairs of nearby points were averaged, and the averages used for calculating intervals and slopes. These averaged points are shown as open circles in Fig. 6

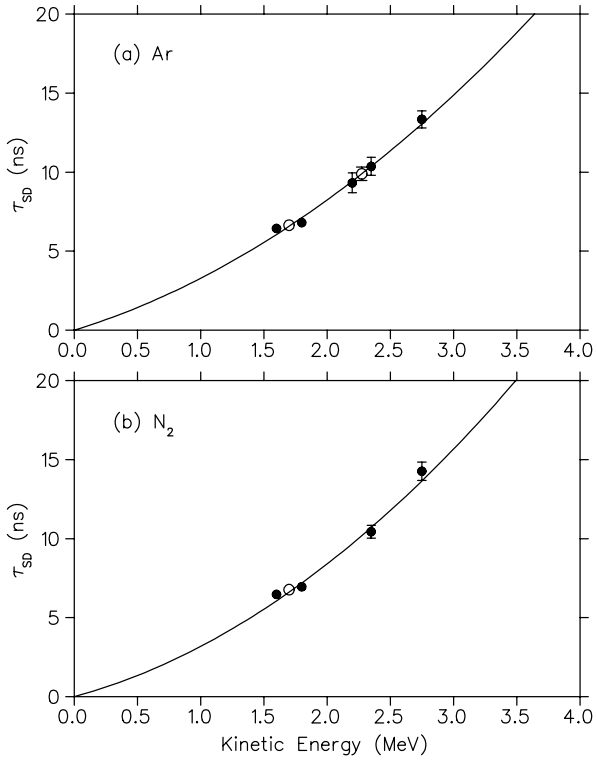

FIG. 6. A plot of the experimental slowing down times at 1 atm, τ_{SD}, vs the measured initial energy, E_i, for Ar (a) and N_2 (b). Error bars on energy are not shown, but are expected to be less than the widths given in Table I. The solid circles are data from Table I and the open circles are the averages of nearby points; these average values were used for calculating the stopping power per molecule, $S(E)$, by finite differences. The solid curves are a quadratic parametrization whose slope was also used to calculate $S(E)$, as described in the text.

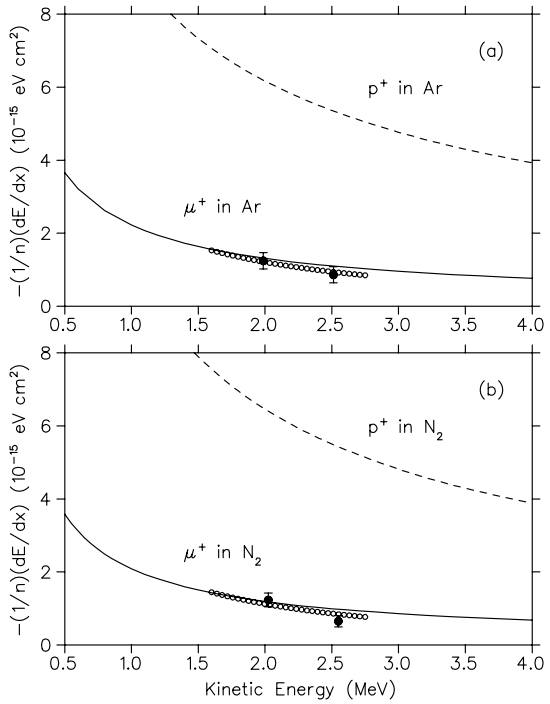

FIG. 7. The stopping power per molecule for the positive muon in Ar (a) and N_2 (b) determined by the slope of τ_{SD} vs E_i. The solid circles with error bars represent measured values obtained from energy intervals while the chains of open circles were determined from the smooth curves in Fig. 6. The dashed lines are the stopping powers for the proton [40,69], at the same energies, E_i. The solid lines, which represent $S(E)=-(1/n)(dE/dx)$ for the positive muon, are obtained by horizontally scaling the energies (mainly off scale) of the proton stopping-power data by 0.11, the ratio of p^+ to μ^+ velocities. There are *no* other adjustments. Such a simple scaling is expected to be inaccurate at the lowest energies plotted, but the agreement is excellent over the range of measured stopping powers.

while the measured points are smaller filled circles. After averaging those pairs, there are three distinct E_i values for both N_2 and Ar, and thus two discrete, reasonably spaced, energy intervals for calculating slopes. The stopping powers calculated from Eq. (26) over these intervals, at their midpoint energies (E_i), are listed in Table III, along with those at the equivalent proton energy, and are shown as solid circles in Fig. 7. The error bars are determined from the uncertainties in τ_{SD} in Table I. There are no horizontal (energy) errors shown, because these were not determined, but, as commented earlier, are estimated to be $\approx$0.1 MeV. The stopping powers for H_2 and 50% H_2-He mixtures were determined over a single interval, 1.1 to 1.6 MeV, with the results also given in Table III. These are essentially the same values, in agreement with the Bethe-Bloch formula, Eq. (1). The corresponding stopping power for protons of the same velocity (12 MeV) in H_2 agrees with literature values, within errors [40].

The second approach to calculating $d\tau_{SD}/dE_i$ was to parametrize the τ_{SD} vs E_i dependence to the quadratic expression $\tau_{SD}=aE_i+bE_i^2$, with phenomenological parameters a and b determined by χ^2 minimization [36]. This parametrization is shown in the smooth curves of Fig. 6, for Ar and N_2, which are the most complete data sets. The slope $d\tau_{SD}/dE_i=a+2bE_i$ and corresponding stopping powers were then calculated for both gases over the energy interval $E_i=1.6$ to 2.8 MeV, as shown by the chains of small circles in Fig. 7. Error bars are not shown but can be expected to be similar to those plotted for the two data points shown.

Figure 7 also plots, as dashed lines, the known proton stopping powers per molecule at the energies given on the abscissa [40,41,69]. The solid lines are the proton data (from energies that are off scale) after compressing the energy scale by a factor of $E_p/E_\mu=m_p/m_\mu=8.88$ (as in the last column of Table III), which then shows the *expected* $S(E)$ for the positive muon based on the assumption of velocity scaling; i.e., the stopping power of the proton and muon in a given medium should be the same at the same projectile *velocity* (speed), as described earlier. There is no further adjustment to the solid lines in Fig. 7, other than the assumption of velocity scaling. Though there is some scatter in the individual comparisons shown in Table III, the agreement with the experimental μSR points, both those determined from the parametrized fits in Fig. 6 (open circles) and the results obtained directly from the intervals, as described above, is good. The apparent drift to fall below the velocity-scaled solid line at the higher energies, occurring for both N_2 and

TABLE III. Stopping powers for μ^+ determined at the midpoints (E_i) of discrete energy intervals, compared with values for p^+.

Gas	E_i interval	mid E_i[a]	$S_\mu(E_i)$[b]	$S_p(8.88E_i)$[c]
Ar	1.70–2.28	2.00	1.24±0.22	1.31
Ar	2.28–2.75	2.51	0.86±0.22	1.10
N_2	1.70–2.35	2.03	1.23±0.19	1.18
N_2	2.35–2.75	2.55	0.65±0.16	0.98
H_2	1.10-1.60	1.35	0.27±0.03	0.29
H_2-He(1:1)	1.10–1.60	1.35	0.24±0.04	0.28[d]

[a]Midpoints of the energy intervals shown. Energies are in MeV. Uncertainties were not determined, but are expected to be ≈0.1 MeV, whereas the measured energy widths at each nominal energy were ≈0.3 MeV.
[b]Muon stopping powers per molecule, $S(E)=-(1/n)(dE/dx)$, in units of 10^{-15} eV cm^2.
[c]Velocity-scaled proton stopping powers, in the same units [40,69] (for a given velocity, $E_p=8.88E_\mu$).
[d]Average of H_2 and He stopping powers [40].

Ar, and visible in both the smoothed and discrete data, suggests a small systematic uncertainty in energy, commented on earlier. While the velocity scaling between the p^+ and μ^+ seen in Fig. 7 is expected from the Bethe-Bloch equation, Eq. (1) [1,25], this is the *first* time, to our knowledge, that it has actually been demonstrated for (~2 MeV) *muons*, in the gas phase.

While, as remarked at the outset (Sec. II A), the much lighter muon mass could, in principle, provide a more stringent test of velocity scaling (or, equivalently, mass independence) in the BB slowing-down formula, this statement has to be weighed against the errors found in a given measurement; and, in particular, with those reported elsewhere in comparisons of p and d stopping powers (in metals) at the same velocities [23–25], with errors at the 0.5% level, or better. The measurements of Shiomi-Tsuda *et al.* are noteworthy here, with (average) errors of 0.35% reported over a wide range of elements, from Be to Au [23]. (It can be commented that similar measurements in gases, by the same group, report 0.8% errors [41].) Though not an issue in the present study, a relevant question to ask is "to what level of error should measurements of muon stopping powers be made in order to provide a better test of mass independence than has been shown by comparative measurements of proton and deuteron stopping powers?"

An answer to this question is provided by the calculations of Bichsel and Inokuti, who have considered specific mass-dependent corrections to the basic electronic stopping-power formula [25]. There are two such corrections, one that is both charge and energy dependent and one that is not, but both of which vary linearly with inverse mass, serving to *decrease* the stopping power for lighter mass particles. Though these calculations are for metal targets (Al and Au), we can assume that the trends reported will be similarly correct in a gas environment, and in particular their results for Al best matches the total charge for our results for muon stopping powers in N_2 and Ar. From Ref. [25] specific mass corrections to the BB formula for a 1 MeV proton (in Al) are 0.026%, and, for the equivalent velocity muon, at 0.113 MeV, 0.23%. (These corrections are both about ten times higher in Au.) For a 1.13-MeV μ^+ and an equivalent velocity 10-MeV p^+, in the BB regime, and well above the CE regime, these same corrections are 0.1% and 0.01%, respectively.

Thus, not only would the proton-deuteron data have to be measured to a level of better than ~0.05% (roughly ten times more precise than current data), but the muon data, though with an allowable error tenfold larger, would have to measured at the 0.1% level, which is out of the question for any experiments in the gas phase. The current measurements are closer to the 20% level (Table III) due both to errors in the measurement of the phase of the Mu precession (Figs. 3 and 4) and uncertainties in the energy of the incident surface μ^+ beam, and as such fall far short of any test of mass independence in the classic BB formula. On the other hand, it may be possible, with current improvements in "slow" μ^+ beams [1,2] (at few "keV" energies) to begin to test such specific mass dependences in muon stopping powers. Indeed, Valdés *et al.* have shown for 0.25 keV muons in Al, that differences with (2.2 keV) proton stopping powers begin to approach the 5% level [22].

Finally, it should be remarked that, although the solid curves for the velocity-scaled stopping powers, $S(E)$, are displayed at quite low muon energies in Fig. 7, velocity scaling is likely to be less valid there, as other mechanisms such as nuclear stopping [22,25,51,70] charge exchange [40,43,49,70], and the Barkas effect [4,5,50] can all contribute to the stopping power at these energies. At the higher energies, the velocity-scaled solid curves are relevant to the 4.1 MeV nominal energy of surface muons [67].

C. Calculations of τ_{SD} in the BB and CE regimes

As outlined in Sec. II B, the survival probability that the positive muon (proton) at initial energy E_i (time $t=0$ and velocity v_i) does *not* undergo an electron capture collision down to some lower energy E (t and v) is expressed by an equivalent form to Eq. (7), $S_C=\exp[-N_C(E_i,E)]$, but involving the ion stopping power $(dE/dx)_+$ in Eq. (8). Figure 8 shows this survival probability for the *proton* in He, Ne, and Ar with $E_i=100$ MeV, calculated from electron capture cross sections [30,71,72] and proton stopping powers [69] in He, Ne, and Ar. The *mean* energy for the first neutral (Mu or H) formation $\langle E_{CE}\rangle$ (defining the beginning of the charge

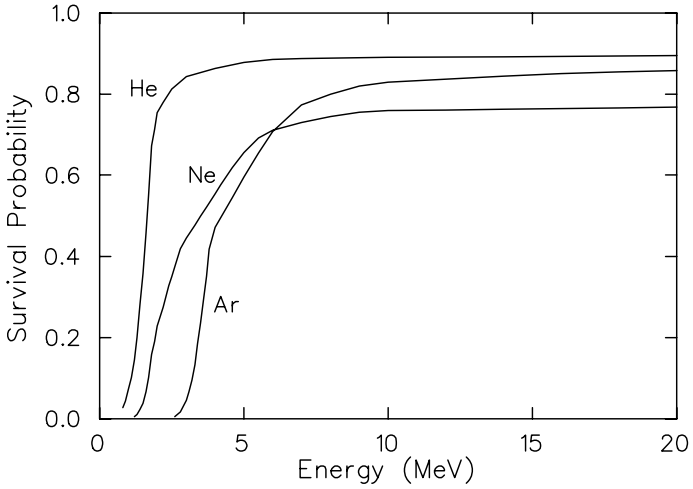

FIG. 8. The survival probability of the proton to the electron capture process (H atom formation) in He, Ne, and Ar with E_i=100 MeV, $S_C(E_i,E)=\exp[-N_C(E_i,E)]$. The mean energy for the first H formation, $\langle E_{CE}\rangle$, can be obtained from the condition $N_C(E_i,\langle E_{CE}\rangle)=1$, i.e., $S_C(E_i,\langle E_{CE}\rangle)=0.368$, to be $\langle E_{CE}\rangle$=1.5, 2.5, and 3.7 MeV in He, Ne, and Ar, respectively.

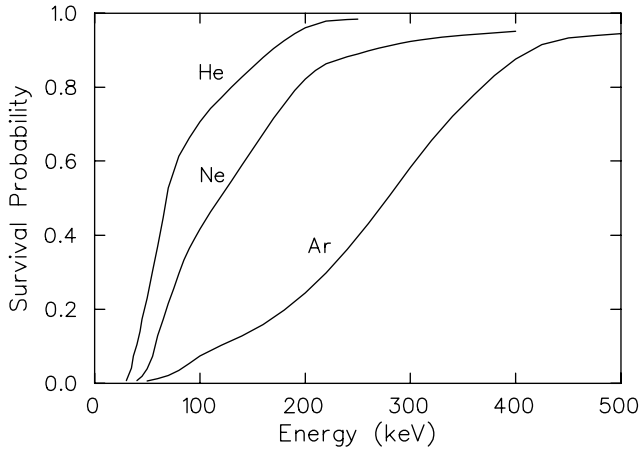

FIG. 9. The survival probability of the positive muon to electron capture (muonium formation) in He, Ne, and Ar with E_i=4 MeV, the energy of a surface muon beam. The mean energies of the first Mu formation are $\langle E_{CE}\rangle$=60, 90, and 240 keV in He, Ne, and Ar, respectively. The calculated values are insensitive to initial energies $\gtrsim$4 MeV.

exchange regime) is obtained from the condition $N_C(E_i,\langle E_{CE}\rangle)=1$, giving $\langle E_{CE}\rangle$=1.5, 2.5, and 3.7 MeV, respectively, which are quite insensitive to the choice of E_i as long as $E_i \gg E_{CE}$. The trend to higher $\langle E_{CE}\rangle$ with increasing Z_T is in accord with the trends seen from proton CE data in the MeV regime [71,73–75], and due, in part, to the contributions from inner shell electrons to $\sigma_C(E)$ at higher energies.

In the case of the positive muon in He, Ne, and Ar, the cross sections for muonium formation, $\sigma_C(E)$, and the stopping power, $(dE/dx)_+$, are obtained by velocity scaling from the corresponding quantities for the proton [30]. The velocity scalability of $\sigma_C(E)$ for the muon is expected at high enough energies [62], and is well established [76], as is that for dE/dx [1,25,23], and seen also in this work (Fig. 7). Figure 9 shows the survival probability for the positive *muon*, with E_i=4 MeV down to energy E in He, Ne, and Ar. The initial energy of 4 MeV was chosen because it is the nominal surface μ^+ beam energy and is again well above the energies of significant Mu atom formation ($E_i \gg E_{CE}$). The mean energies of the first muonium formation calculated from the velocity-scaled cross sections are $\langle E_{CE}\rangle$=60, 90, and 240 keV in He, Ne, and Ar, respectively. The trend to considerably reduced value for $\langle E_{CE}\rangle$ compared to those for the proton above, partly reflects the mass dependence inherent to the survival probability, from Eqs. (7) and (8), though, in fact, there is no simple mass relationship.

The time in the Bethe-Bloch regime, t^+_{BB}, can be found from the stopping power for this regime by Eq. (6), with $E_f=\langle E_{CE}\rangle$, the average energy at which the first muonium (hydrogen) formation collision takes place. As an example calculation, consider argon. The slowing-down time of the μ^+ through the BB regime, from an initial energy of E_i=2.8 MeV, the highest value in the present study (Table I), to 240 keV, the beginning of the charge exchange regime ($\langle E_{CE}\rangle$, as above), was calculated from the corresponding velocity-scaled proton stopping powers of Ref. [69] (very similar, where comparable, to those reported earlier by Andersen and Ziegler [39], by Bichsel and Porter [40], and more recently by Shiomi-Tsuda *et al.* [41]), giving t^+_{BB} (Mu)=12.3 ns at 1 atm pressure. This compares favorably with an earlier, more simplistic estimate in the range 3 MeV to 35 keV of 14 ns [16] and more importantly with the measured slowing-down time to $\approx$10 eV, τ_{SD}=13.3±0.5 ns (Table I), indicating that the μ^+ spends 1.0±0.5 ns in the cyclic CE regime, spanning energies from about 240 keV to 10 eV (in Ar).

Specific calculations of muon SD times *in* the CE regime [28], using velocity scaling of the (proton) CE cross sections and energy scaling for the elastic moderation cross sections, showed that it takes ~0.2 ns to slow muons in (1 atm) Ar from 2 keV to 10 eV, the energy region in the CE regime where most muon depolarization takes place. Extending the upper energy of these calculations to 240 keV can be expected to lengthen this time, consistent with the 1.0 ns above. It is worth commenting that, even though the total time in the cyclic charge exchange regime (~1.0 ns) is much longer than the muonium hyperfine period $2\pi/\omega_0$=0.224 ns, each *individual* Mu residence time is much shorter. This allows most of the muon spin polarization to be preserved at observation times, after thermalization, at pressures $\gtrsim$1 atm, in all but the heaviest gases [11,16,28,48,63].

D. τ_{SD} in gas mixtures: Bragg's rule

In the Bethe-Bloch formula of Eqs. (1) and (3), the stopping power dE/dx is linearly proportional to nZ_T, which is the total electron density of the target. Furthermore, as just shown, $t^+_{BB} \gg t_{CE}$, justifying the earlier approximation that $t_{SD} \approx t_{BB}$. Thus the quantity $\tau_{SD}Z_T$ is a measure of the slowing-down time *per electron* in the moderator (at 1 atm

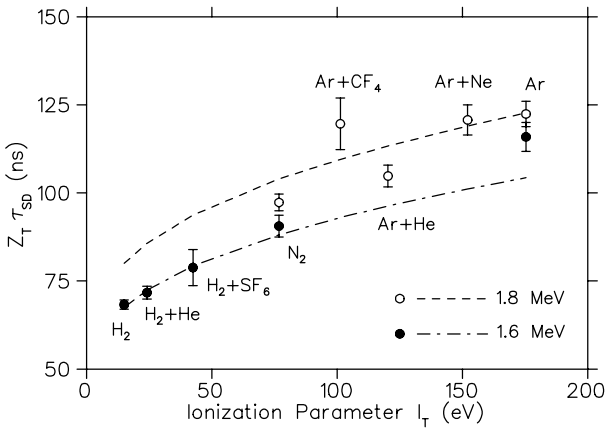

FIG. 10. The product of the slowing-down time and the total charge of the moderator, $\tau_{SD}Z_T$, which is a measure of the slowing-down time per electron in the gas, for all the gases and mixtures in Tables I and II with initial muon energies E_i=1.6 (solid circles) and 1.8 MeV (empty). The corresponding dot-dashed and dashed lines are not fits, but were calculated from Eq. (28), as described in the text.

and 300 K) through the BB regime. This is plotted in Fig. 10 as a function of I_T in pure gases and in gas mixtures, for initial muon energies E_i=1.6 MeV (solid circles) and 1.8 MeV (open circles), where the times τ_{SD} are taken from Tables I and II. The curves are calculated from the Bethe-Bloch formula, as described next.

In the approximation $t_{SD} \approx t_{BB}^{+}$, one can express $t_{SD}Z_T$ using Eqs. (3) and (6) as

$$t_{SD}Z_T = \frac{m_e m}{4\pi e^4 z_p^2 n}\int_{v_f}^{v_i} \frac{v^2 dv}{\ln(2m_e v^2/I_T)}, \tag{27}$$

where v_f is the velocity at which the first electron capture takes place, corresponding to $\langle E_{CE}\rangle$, as defined above, and the quantities Z_T and I_T for mixtures are calculated from Eqs. (4) and (5), respectively. The values determined for I_T are found from those given in Ref. [52] as shown by the entries along the abscissa of Fig. 10, and which are in reasonable agreement with other literature values [40,41]. The expression for $t_{SD}Z_T$ given by Eq. (27) can be cast in the form

$$t_{SD}Z_T = \frac{m_e m}{8\pi e^4 z_p^2 n}\left(\frac{I_T}{2m_e}\right)^{3/2}[H(v_i) - H(v_f)], \tag{28}$$

where

$$H(v) = \mathrm{Li}([2m_e v^2/I_T]^{3/2})$$

is a convenient notation, and where Li(x) is the *integral logarithm* defined by [77]

$$\mathrm{Li}(x) = \int_0^x \frac{dt}{\ln t} = \ln\ln x + \sum_{j=1}^{\infty}\frac{(\ln x)^j}{jj!}.$$

Calculations of $\tau_{SD}Z_T$ from Eq. (28), for muon energies E_i=1.6 and 1.8 MeV and E_f = 0.4 MeV, are shown by the dashed curves in Fig. 10. Though some differences may be expected for a different choice of I_T values, which can show $\gtrsim$10% variation in the literature [40,41,52], the calculated curves do nicely follow the trend of the measured points, with an average deviation of about 20%, typical of other reported tests of Bragg's rule [53,59]. Notable exceptions are the 50% deviations reported in H_2-He mixtures at keV energies, due to charge-changing collisions [54] and a 5% level recently reported in polymers using the Sigmund-Schinner binary collision theory [45]. The generally good agreement seen in Fig. 10 does indeed indicate that each electron in a molecule or mixture has essentially the same contribution to the slowing-down time as an electron in a pure atomic gas, in accord with the validity of Bragg's additivity rules of Eqs. (4) and (5), but not previously shown experimentally for the μ^+ in gases.

VII. THERMALIZATION REGIME AND TOTAL SLOWING-DOWN TIME

After emerging from charge exchange, the muon (proton) enters a final thermalization regime, from the energy of the last Mu (H) formation, at ~10 eV, to kT. In a noble gas, this energy loss is almost exclusively due to elastic scattering, but in molecular gases, inelastic scattering via rovibrational excitation also plays an important role, in competition with reactive scattering in the form of hot atom reactions of muonium, Mu* [13]. The formalism developed in Ref. [13] is also relevant to the slowing-down time in the thermalization regime here, and is outlined below.

A. Energy moderation and the final thermalization time, τ_{TH}

When the kinetic energy of the projectile in the thermalization regime is well above thermal, the *elastic* energy-loss parameter $f_0(E)$ in Eq. (9) can be expressed by [13,26]

$$f_0(E) = \frac{1}{\sigma(E)}\int\left(\frac{d\sigma(E,\theta)}{d\Omega}\right)\left[1 - \frac{2Mm}{(M+m)^2}(1-\cos\theta)\right]d\Omega, \tag{29}$$

where $d\sigma(E,\theta)/d\Omega$ and $\sigma(E)$ are the angular-differential and angular-integrated elastic cross sections, respectively. The normalized angular distribution can be expressed in terms of a sum over Legendre polynomials, with expansion coefficients $s_n(E)$. Because of the orthogonality of these polynomials, the stopping power contains no terms with $n \geq 2$ [13]. The "monopole" coefficient $s_0(E)$ is identically unity, while the "dipole" coefficient, $s_1(E)$, is a measure of the forwardness in the angular distribution for elastic scattering, and can be represented as the average of the center-of-mass (CM) scattering angle, $s_1(E) = \langle\cos\theta\rangle$.

Thus, the stopping power of the *elastic* energy-moderation process of Eq. (9) can be expressed by

$$\left(\frac{dE}{dx}\right)_{\mathrm{Elastic}} = \ln\left(1 - \frac{2Mm}{(M+m)^2}[1 - s_1(E)]\right)En\sigma(E), \tag{30}$$

since the quantity $I_0(E)$ vanishes for elastic collisions. If the scattering is isotropic in the CM system, the dipole coeffi-

cient $s_1(E)$ vanishes as well, and gives the familiar result for hard spheres; whereas $s_1(E)=1(-1)$ represents, classically, completely forward (backward) scattering. Note that dE/dx in this regime can be drastically reduced from that for hard spheres, by the factor $1-s_1(E)$, depending on how forward peaked the elastic differential cross sections are. Related effects for heavy ions have also been considered by Sørensen [78]. As noted, in the case of molecular gases, inelastic (rovibrational) excitation may also be important in the energy moderation process (including in the BB regime, pointed out earlier in comparing the similar times τ_{SD} in H_2 and D_2) and a form similar to Eq. (30) can also be defined by its forwardness scattering parameter [13].

The stopping-power expression of Eq. (30) assumes that the target gas atoms are at rest, which is a good approximation for E much greater than thermal energy, $E_T=3/2kT$, but at lower energies the thermal motion of the target must be taken into consideration [79]. In this case, the stopping power due to elastic collisions is modified to

$$\left(\frac{dE}{dx}\right)_{\text{Elastic}} = \ln\left[1-\frac{2Mm}{(M+m)^2}\left(1-\frac{E_T}{E}\right)[1-s_1(E)]\right]nE\sigma(E). \tag{31}$$

This expression is valid as long as $\sigma(E_+)\approx\sigma(E_-)$, where $E_\pm=\frac{1}{2}m(v_p\pm v_T)^2$ are the maximum and minimum relative kinetic energies in terms of the projectile and target velocities. The stopping power given by Eq. (31) is negative for $E>E_T$ ("cooling") and vice versa ("heating"), indicating that the final average energy of the projectile is $3kT/2$, regardless of the initial energy.

In order to estimate the rate of energy loss in the thermalization regime, i.e., *after* the last CE cycle, the quantities $\sigma(E)$ and $s_1(E)$ considered in Eq. (31) are replaced by average values $\langle\sigma\rangle$ and $\langle s_1\rangle$, respectively. The slowing-down time from $E_{\max}=\alpha E_T$, the initial energy immediately following CE (about 10 eV) to $E_{\min}=\beta E_T$ is then given by

$$t(\alpha E_T,\beta E_T)=\frac{\tau_0}{2}\left[\ln\left(\frac{\sqrt{\beta}+1}{\sqrt{\beta}-1}\right)-\ln\left(\frac{\sqrt{\alpha}+1}{\sqrt{\alpha}-1}\right)\right], \tag{32}$$

where α and β are dimensionless scale factors for energy ($\alpha>\beta>1$), and τ_0 is a characteristic thermalization time defined by

$$\tau_0=\frac{(M+m)^2}{Mm}\frac{1}{n\langle\sigma\rangle(1-\langle s_1\rangle)}\sqrt{\frac{m}{2E_T}}, \tag{33}$$

where n is again the molecular number density. Figure 11 plots results from Eq. (32), showing energy losses as a function of time relative to τ_0 (solid lines) for initial energies $\alpha E_T=2E_T$, $5E_T$, and $258E_T$ (10 eV). Note the correct asymptotic result at long times ($E\to E_T$), which is in contrast to the dotted line, for an initial energy of 10 eV, calculated from Eq. (30), which ignores the thermal motion of the target.

To calculate specific times, knowledge of both the average cross sections and dipole parameters are required. As a simple estimate, assuming a cross section of $\langle\sigma\rangle=10^{-15}$ cm^2, and $\langle s_1\rangle=0$, the case for (classical) *isotropic* hard spheres, the thermalization time of Mu in Ar at 1 atm pressure and 300 K, from 10 eV down to $2E_T=3kT\sim0.1$ eV, would be $\tau_{TH}\approx20$ ns, consistent with earlier calculations of the same quantity [16]. [Similar considerations also apply to electron and positron scattering, where the quantity $s_1(E)$ for the elastic process vanishes (in Ar) at approximately 1 eV and below [80]]. For H_2, assuming the same cross section and energy regime, the large reduction in mass of the target molecule, compared to Ar, would naturally mean a much faster Mu thermalization, with $\tau_{TH}\approx1$ ns for isotropic scattering, at pressures near 1 atm.

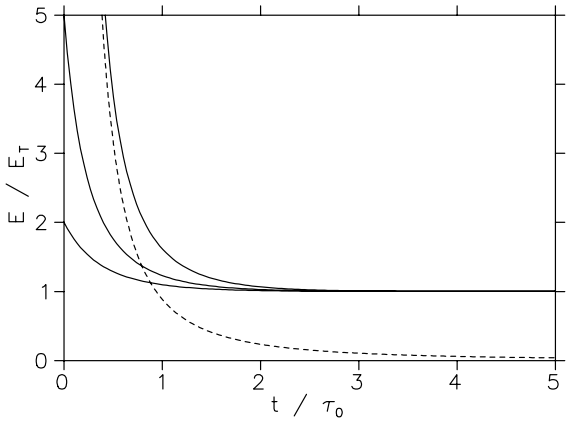

FIG. 11. Thermalization towards $E_T=\frac{3}{2}kT$, plotting the energy ratio $E/E_T=\alpha$ vs t/τ_0, where τ_0 is the characteristic time defined in Eq. (33). The three solid lines are for initial energies $2E_T$, $5E_T$, and $258E_T$ (10 eV). The dotted line, also for 10 eV, is based by Eq. (30), which ignores thermal motion of the target.

However, as mentioned above, the actual slowing down time can be *much* longer, depending on the scale factor for the forwardness in the elastic differential cross sections, $1/[1-\langle s_1\rangle]$. A detailed scattering calculation is required to determine this which has been done to date only for Mu^* reactions with H_2, from calculated QCT differential cross sections [13]. Choosing an average value for $\langle\sigma\rangle$ of 2×10^{-15} cm^2 from these calculations, again from 10 eV down to $2E_T$, as above, and an average value for $\langle s_1\rangle=0.95$ in this energy range, gives a time $\tau_0\approx10$ ns and hence, from Fig. 11, a thermalization time to $\lesssim0.1$ eV, $\tau_{TH}\approx9$ ns, an order of magnitude longer than the hard-sphere estimate above. Extending this calculation even nearer to thermal energies [$\beta\to1$ in Eq. (32)], would mean $\tau_{TH}\approx30$ ns in H_2 at 1 atm pressure. In Ar, with its much higher mass, and assuming the same parameters, the time to reach thermal energies could be an order of magnitude longer, but the actual scattering calculations for the Mu atom have not been performed. Still, the trend is noteworthy and could extend to much longer times in the heavy noble gases, Kr and Xe [63]. On the other hand, in these cases the (H atom) elastic scattering cross sections are some twofold to threefold larger [81], and inelastic (electronic) excitation would likely be more pronounced, arguing for shorter slowing times than those based on elastic scattering alone.

B. Total slowing-down times and μSR measurements

Knowledge of the slowing-down times for positive muons and muonium is important in two major aspects pertaining to

μSR studies: the time scale for radiolysis effects and radiation chemistry in dense media [6,8–10,20,21,37], and the time scale for prompt vs thermal reactions in the gas phase. In the first instance it is the *total* time, τ_{TOT}, that is most relevant; in the second it is primarily the final thermalization time, τ_{TH}.

Since $\tau_{TOT}=\tau_{SD}+\tau_{TH}$, where τ_{SD} is the measured slowing-down time of the μ^+ through the BB (mainly) and CE regimes ($\sim$10 ns at 1 atm pressure for muon energies $E_i \approx 2$ MeV, Tables I and II), τ_{TOT} can be expected to be dominated by τ_{TH}, the time in the final thermalization regime, as $3/2kT$ is approached. As previewed above, for the noble gases He, Ne, and Ar, where only elastic scattering would be important in the energy regime of interest, one could expect this time to vary from tens of ns to perhaps hundreds of ns near 1 atm, depending on target mass and both the magnitude and forwardness of the differential cross sections, which are not known for the Mu atom. For molecular gases like H_2, inelastic (rovibrational) scattering will serve to shorten thermalization times due to elastic scattering alone, where τ_{TT} is $\approx$30 ns in 1 atm H_2. Higher pressures will also naturally give rise to shorter slowing-down times, so it is reasonable to expect a total stopping time to *thermal* energies (E_T) of $\tau_{TOT} \approx \tau_{TH} \lesssim 100$ ns in most gases at pressures near 1 atm. Times of this order are consistent with recent pulsed-beam rf measurements in the gases Ne, Ar, N_2, and Kr, where no formation of either Mu or of diamagnetic species (MMu^+ molecular ions) was observed beyond the 80 ns width of the beam pulse [11].

Knowledge of Mu thermalization times, τ_{TH}, is most important for the proper interpretation of *thermal* reaction rates in the study of gas-phase Mu chemistry and reaction kinetic [12,31,32,65]. Incomplete thermalization would be of particular concern in the study of endothermic reactions such as $Mu+H_2(D_2)$ [31] and $Mu+CH_4$ [33,65] where the reaction rate varies strongly with temperature, and, by implication, with any contributions from nonthermal reactions. Since moderators utilized in Mu chemistry studies, necessary to produce Mu by the CE processes discussed above, are typically Ar or N_2 at pressures $\gtrsim$1 atm, or other molecular gases where rovibrational (inelastic) scattering will be more important, we can expect thermalization times consistent with the $\lesssim$100 ns estimate above. The $Mu+H_2$ reaction is the best test case of this, since, in addition to being endoergic, comparisons of reaction rates with essentially exact theoretical calculations (on the Liu-Siegbahn-Truhlar-Horowitz potential energy surface) [82] show exemplary agreement between theory and experiment [31]. Were τ_{TH} to be appreciably longer, this would not be the case.

VIII. SUMMARY

The slowing-down times of energetic positive muons, from initial energy E_i (0.9 to 2.8 MeV), through the Bethe-Bloch and charge-exchange regimes (down to $\approx$10 eV, in Ar), have been determined from measurements of the initial phase, ϕ_{Mu}, of the Mu precession signal, in μSR experiments. These times, τ_{SD}, fall in the range $\sim$5–35 ns (at 1 atm and 300 K) and are typically faster at lower incident energies and in molecules (and mixtures) of higher charge densities. Comparisons of slowing-down times for molecules and mixtures indicate that Bragg's additivity rule is also quite well obeyed for stopping muons, at the 20% level of accuracy that the present experiments allow.

The technique also allows a determination of the μ^+ stopping power per molecule, $S(E)=-(1/n)(dE/dx)$, described by the historic Bethe-Bloch equation. In Ar, N_2, H_2, and in a H_2-He mixture, $S(E)$ for the positive muons agrees, within errors, with those known for the proton at the *same speed*, as expected from "velocity scaling" of the Bethe-Bloch formula in the MeV energy regime. Though this is not a surprising result, the present measurements of μ^+ stopping powers in gases, are, in fact, the first of their kind to our knowledge.

However, the ($\sim$20%) errors in the measurement of $S(E)$ for the muon, arising from uncertainties both in the Mu precession phase, ϕ_{Mu}, and in the energies of the incident muon beam, preclude any test of a specific mass dependence in the classic stopping power formula. In principle, this can be more sensitively tested by the muon than the proton [25], but the level of precision required is at the 0.1% level, which simply cannot be obtained in a gas phase measurement. Even very precise earlier measurements of proton and deuteron stopping powers in metals, at the 0.5% level [23,24] are still too imprecise for such a test, by an order of magnitude [25].

In addition to the experimental results, calculations of the average energy for the onset of charge exchange, $\langle E_{CE} \rangle$, and the separate times spent in the Bethe-Bloch ($\sim$10 ns) and charge-exchange ($\sim$1 ns) regimes are also presented. This formalism has also been extended to calculations of the final thermalization time, τ_{TH}, i.e., after the charge-exchange regime, from the energy of the last muonium formation ($\approx$10 eV) down to thermal energy. This final thermalization time depends critically on the dipole (forwardness) parameter, $s_1(E)$, for elastic scattering, which can markedly increase the thermalization time of μ^+/Mu in the few-eV regime, beyond hard sphere expectations. Total slowing-down times of energetic (MeV) muons in most gases are dominated by τ_{TH} and are expected to be $\lesssim$100 ns at nominal pressures. This time is important to the proper interpretation of thermal rate constants for Mu reactivity, and, along with τ_{SD} measured in the Bethe-Bloch and charge-exchange regimes, is important also to an estimation of time scales for prompt processes in muon radiolysis studies.

[1] E. Morenzoni, H. Glückler, T. Prokscha, R. Khasanov, H. Luetkens, M. Birke, E. M. Forgan, Ch. Niedermayer, and M. Pleines, Nucl. Instrum. Methods Phys. Res. B **192**, 254 (2002).
[2] T. Prokscha, E. Morenzoni, N. Garifianov, H. Glücker, R. Khasanov, H. Luetkens, and A. Sutter, Physica B **326**, 51 (2003).
[3] F. Mulhauser, J. L. Beveridge, G. M. Marshall, J. M. Bailey, G. A. Baer, P. E. Knowles, G. R. Mason, A. Olin, M. C. Fujiwara, T. M. Huber, R. Jacot-Guillarmod, P. Kammel, Z. Zmeskal, S. K. Kim, A. R. Kunselman, V. E. Markushin, C. J. Martoff, and C. Petitjean, Phys. Rev. A **53**, 3069 (1996).
[4] L. H. Andersen, P. Hvelplund, H. Knudsen, S. P. Møller, J. O. P. Pedersen, E. Uggerhøj, K. Elsener, and E. Morenzoni, Phys. Rev. Lett. **62**, 1731 (1989).
[5] R. Schmidt, H. Daniel, F. J. Hartmann, P. Hauser, F. Kottmann, M. Mühlbauer, C. Petijean, W. Schott, D. Taqqu, and P. Wojciechowski, Eur. Phys. J. D **3**, 119 (1999).
[6] G. A. Salmon, Physica B **326**, 46 (2003).
[7] E. Roduner, in *Radiation Chemistry: Present Status and Future Prospects*, edited by C. D. Jonah and B. S. M. Rao (Elsevier, Amsterdam, 2001).
[8] A. Mozumder, *Fundamentals of Radiation Chemistry* (Academic Press, London, 1999).
[9] D. C. Walker, *Muon and Muonium Chemistry* (Cambridge University Press, Cambridge, 1983).
[10] K. Ghandi, M. Bridges, D. J. Arseneau, and D. G. Fleming, J. Phys. Chem. A **108**, 11613 (2004).
[11] C. Johnson, S. P. Cottrell, K. Ghandi, and D. G. Fleming, J. Phys. B **38**, 119 (2005).
[12] J. J. Pan, D. J. Arseneau, M. Senba, D. G. Fleming, U. Himmer, and T. Suzuki, Phys. Chem. Chem. Phys. **2**, 621 (2000).
[13] M. Senba, D. G. Fleming, D. J. Arseneau, and H. R. Mayne, J. Chem. Phys. **112**, 9390 (2000).
[14] D. G. Fleming and M. Senba, in *Perspectives of Meson Science*, edited by T. Yamazaki, K. Nakai, and K. Nagamine (North Holland, Amsterdam, 1992), p. 219.
[15] D. G. Fleming, M. Senba, J. J. Pan, and D. J. Arseneau, in *The Physics of Electronic and Atomic Collisions XIX International Conference, Whistler BC, 1995*, edited by L. J. Dubé, J. B. A. Mitchell, J. W. McConkey, and C. E. Brion, *AIP Conf. Proc. No. 360* (AIP, New York, 1995), p. 413.
[16] D. G. Fleming, R. J. Mikula, and D. M. Garner, Phys. Rev. A **26**, 2527 (1982).
[17] D. G. Fleming, R. J. Mikula, M. Senba, D. M. Garner, and D. J. Arseneau, Chem. Phys. **82**, 75 (1983).
[18] D. J. Arseneau, D. G. Fleming, M. Senba, I. D. Reid, and D. M. Garner, Can. J. Chem. **66**, 2018 (1988).
[19] M. Senba, D. G. Fleming, D. J. Arseneau, D. M. Garner, and I. D. Reid, Phys. Rev. A **39**, 3871 (1989).
[20] P. W. Percival, J-C. Brodovitch, K. Ghandi, B. A-Jones, J. Schüth, and D. M. Bartels, Phys. Chem. Chem. Phys. **1**, 4999 (1999).
[21] D. G. Eshchenko, V. Storchak, J. H. Brewer, G. D. Morris, and S. S. J. Cox, Phys. Rev. B **66**, 035105 (2002).
[22] J. E. Valdés, P. Vargas, and N. R. Arista, Nucl. Instrum. Methods Phys. Res. B **174**, 9 (2001).
[23] N. Shiomi-Tsuda, N. Sakamoto, and R. Ishiwari, Nucl. Instrum. Methods Phys. Res. B **93**, 391 (1994).
[24] H. H. Andersen, J. F. Bak, H. Knudsen, and B. R. Nielsen, Phys. Rev. A **16**, 1929 (1977).
[25] H. Bichsel and M. Inokuti, Nucl. Instrum. Methods Phys. Res. B **134**, 161 (1998).
[26] M. Senba, J. Phys. B **21**, 3093 (1988).
[27] M. Senba, J. Phys. B **22**, 2027 (1989).
[28] M. Senba, J. Phys. B **23**, 1545 (1990).
[29] M. Senba, Hyperfine Interact. **65** 779 (1990).
[30] M. Senba, J. Phys. B **31**, 5233 (1998).
[31] I. D. Reid, D. M. Garner, L. Y. Lee, M. Senba, D. J. Arseneau, and D. G. Fleming, J. Chem. Phys. **86**, 5578 (1987).
[32] S. Baer, D. Fleming, D. Arseneau, M. Senba, and A. Gonzalez, in *Isotope Effects in Gas-Phase Chemistry*, edited by J. A. Kaye, *ACS Symposium Series 502.* (American Chemical Society, Washington, D.C 1992) p. 111.
[33] J. Pu and D. G. Truhlar, J. Chem. Phys. **117**, 10675 (2002).
[34] J. R. Kempton, D. J. Arseneau, D. G. Fleming, M. Senba, A. C. Gonzalez, J. J. Pan, A. Tempelmann, and D. M. Garner, J. Phys. Chem. **95**, 7338 (1991).
[35] R. E. Turner, R. F. Snider, and D. G. Fleming, Phys. Rev. A **41**, 1505 (1990).
[36] M. Senba, D. J. Arseneau, A. C. Gonzalez, J. R. Kempton, J. J. Pan, A. Tempelmann, and D. G. Fleming, Hyperfine Interact. **65**, 793 (1990).
[37] D. C. Walker, S. Karolczak, G. B. Porter, and H. A. Gillis, J. Chem. Phys. **118**, 3233 (2003); D. C. Walker, D. Karolczak, H. A. Gillis, and G. B. Porter, Can. J. Chem. **81**, 199 (2003).
[38] S. K. Allison, Rev. Mod. Phys. **30**, 1137 (1958).
[39] H. H. Andersen and J. F. Ziegler, *Hydrogen Stopping Powers and Ranges in all Elements* (Pergamon, New York, 1977).
[40] H. Bichsel and L. E. Porter, Phys. Rev. A **25**, 2499 (1982).
[41] N. Shiomi-Tsuda, N. Sakamoto, H. Ogawa, M. Tanaka, M. Saitoh, and U. Kitoba, Nucl. Instrum. Methods Phys. Res. B **149**, 17 (1999).
[42] G. Reiter, N. Kniest, E. Pfaff, and G. Clausnitzer, Nucl. Instrum. Methods Phys. Res. B **44**, 399 (1990).
[43] P. Sigmund and A. Schinner, Nucl. Instrum. Methods Phys. Res. B **193**, 49 (2002).
[44] K. Bichsel, Phys. Rev. A **65**, 052709 (2002).
[45] S. Damache, S. Ouichaoui, A. Belhout, A. Medouni, and I. Toumert, Nucl. Instrum. Methods Phys. Res. B **225**, 449 (2004).
[46] M. Inokuti, Rev. Mod. Phys. **43**, 297 (1971).
[47] J. R. Kempton, M. Senba, D. J. Arseneau, A. C. Gonzalez, D. M. Garner, and J. J. Pan, J. Chem. Phys. **94**, 1046 (1991).
[48] D. J. Arseneau, D. M. Garner, M. Senba, and D. G. Fleming, J. Phys. Chem. **88**, 3688 (1984).
[49] L. G. Glazov, Nucl. Instrum. Methods Phys. Res. B **95**, 118 (2002).
[50] L. E. Porter, Phys. Rev. A **50**, 2397 (1994); Nucl. Instrum. Methods Phys. Res. B **12**, 50 (1985).
[51] L. G. Glazov and P. Sigmund, Nucl. Instrum. Methods Phys. Res. B **207**, 240 (2003); P. Sigmund and A. Schinner, Nucl. Instrum. Methods Phys. Res. B **195**, 64 (2002); Eur. Phys. J. D **12**, 425 (2000).
[52] J. Oddershede and J. R. Sabin, At. Data Nucl. Data Tables **31**, 275 (1984).
[53] G. Reiter, E. Pfaff, and G. Clausnitzer, Nucl. Instrum. Methods Phys. Res. B **51**, 320 (1990).
[54] R. Golser, D. Semrad, and F. Aumayr, Phys. Rev. Lett. **76**, 3104 (1996).

[55] F. J. Hartmann, H. Daniel, Chr. Maierl, M. Muhlbauer, W. Schott, P. Wojciechowski, P. Hauser, C. Petijean, D. Taqqu, F. Kottmann, and V. E. Markushin, Hyperfine Interact. **101/102**, 623 (1996).
[56] J. R. Sabin, J. Oddershede, and P. Sigmund, Nucl. Instrum. Methods Phys. Res. B **12**, 80 (1985).
[57] H. Paul, Nucl. Instrum. Methods Phys. Res. B **217**, 7 (2004).
[58] Y. J. Xu, G. S. Khandelwal, and J. W. Wilson, Phys. Rev. A **32**, 629 (1985).
[59] P. Bauer, Nucl. Instrum. Methods Phys. Res. B **45**, 673 (1990).
[60] J. F. Ziegler and J. M. Manoyan, Nucl. Instrum. Methods Phys. Res. B **35**, 215 (1988).
[61] H. Ammi, S. Mammeri, M. Chekirine, B. Bouzid, and M. Allab, Nucl. Instrum. Methods Phys. Res. B **198**, 5 (2002).
[62] S. L. Varghese, G. Bissinger, J. M. Joyce, and R. Laubert, Phys. Rev. A **31**, 2202 (1985).
[63] J. R. Kempton, M. Senba, D. J. Arseneau, A. C. Gonzalez, J. J. Pan, A. Tempelmann, D. M. Garner, and D. G. Fleming, Hyperfine Interact. **65**, 801 (1990).
[64] D. G. Fleming, L. Y. Lee, M. Senba, D. J. Arseneau, I. D Reid, and D. M. Garner, Radiochim. Acta **43**, 98 (1988).
[65] R. Snooks, D. J. Arseneau, D. G. Fleming, M. Senba, J. J. Pan, M. Shelley, and S. Baer, J. Chem. Phys. **102**, 4860 (1995).
[66] M. Senba, J. Phys. B **24**, 3531 (1991).
[67] J. L. Beveridge, J. Doornbos, and D. M. Garner, Hyperfine Interact. **32**, 907 (1986).
[68] T. Kusakabe, M. Kimura, L. Pichi, R. J. Buneker, and H. Tawara, Phys. Rev. A **68**, 050701 (2003).
[69] International Commission on Radiation Units and Measurements, ICRU Report No. 49, (1993) (unpublished).
[70] R. Cabrera-Trujillo, Y. Öhrti, E. Deumens, and J. R. Sabin, Phys. Rev. A **62**, 052714 (2000).
[71] Y. Nakai, T. Shirai, T. Tabata, and R. Ito, At. Data Nucl. Data Tables **37**, 69 (1987).
[72] Z. Z. Latypov and A. A Shaporenko, Sov. Phys. Tech. Phys. **21**, 1277 (1976).
[73] C. D. Lin, S. C. Soong, and L. N. Tunnell, Phys. Rev. A **17**, 1646 (1978).
[74] R. D. DuBois and S. T. Manson, Phys. Rev. A **35**, 2007 (1987).
[75] C. L. Cocke, J. R. Macdonald, B. Curmitee, S. L. Varghese, and R. Randall, Phys. Rev. Lett. **36**, 782 (1976).
[76] B. H. Bransden and C. Forster, J. Phys. B **23**, 115 (1990).
[77] I. N. Bronshtein and K. A. Semendyayev, *Handbook of Mathematics*, 3rd ed. (Van Nostrand Reinhold, New York, 1985).
[78] A. H. Sørensen, Phys. Rev. A **55**, 2896 (1997).
[79] J. Park, N. Shafer, and R. Bersohn, J. Chem. Phys. **91**, 7861 (1989).
[80] M. Senba, in *Atomic Physic with Positrons*, edited by J. W. Humberston and E. A.G. Armour (Plenum, New York, 1987), p. 433.
[81] R. W. Bickes Jr., B. Lantzch, J. P. Toennies, and K. Walaschewski, Faraday Discuss. Chem. Soc. **55**, 167 (1973).
[82] K. Tsuda, K. Moribayashi, and H. Nakamura, J. Chem. Phys. **103**, 5512 (1995).